

THE FLORIDA STATE UNIVERSITY
COLLEGE OF ARTS AND SCIENCES

DYNAMICS OF THE NORTH HAWAIIAN RIDGE CURRENT

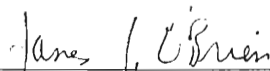
By

ALAN P. LEONARDI

A thesis submitted to the
Department of Oceanography
in partial fulfillment of the
requirements for the degree of
Master of Science

Degree Awarded:
Summer Semester, 1998

The members of the Committee approve the thesis of Alan P.
Leonardi defended on May 15, 1998.



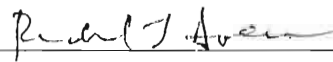
James J. O'Brien
Professor Directing Thesis



William K. Dewar
Committee Member



Harley E. Hurlburt
Committee Member



Richard L. Iverson
Committee Member

Approved:



David Thistle, Chair, Department of Oceanography

Ai miei genitori.

ACKNOWLEDGEMENTS

I would first like to recognize and thank my major professor, the distinguished Dr. James J. O'Brien, for his guidance, inspiration, tutelage, and most of all for allowing me the opportunity to perform this research. Secondly, I would like to thank Dr. Harley E. Hurlburt, my thesis advisor from Naval Research Laboratory (NRL) at Stennis Space Center, Mississippi. Discussions with Dr. Hurlburt have led to many epiphanies regarding ocean dynamics and thesis writing. Also of NRL Stennis Space Center thanks goes to Joe Metzger, Jay Shriver, and Alan Wallcraft for countless hours of help with the model and numerical calculations.

From the Center for Ocean-Atmospheric Prediction Studies (COAPS) at The Florida State University, I would like to thank Dr. Steven Meyers for his editorial help and theoretical discussions, James Stricherz for his computational help, Jordan Yao for his patience in all things computational, and Vince Mariner, Information Specialist, for finding all of the obscure resources required of this research. From The Florida State University department of Oceanography, I would like to thank Dr. Dewar for his help with some of the more dynamical issues of the research.

This research was conducted under Naval Research Laboratory grant N00014-94-1-G918. All research performed was done while the author was an NRL Graduate Research Fellow. This research is a contribution to the 6.1 project on the Dynamics of Low Latitude Western Boundary Currents under program element 61153N sponsored by the Office of Naval Research. The numerical simulations were performed on the Thinking Machines Corporation C90/161024 at the Naval Oceanographic Office sponsored by the Office of Naval Research. The numerical simulations were performed on the Thinking Machines Corporation C90/161024 at the Naval Oceanographic Of-

face, Stennis Space Center, Mississippi, and the Cray CM-5E at NRL Washington, D.C., as part of the Department of Defense (DoD) High Performance Computing Modernization Program (HPCMP).

TABLE OF CONTENTS

LIST OF TABLES	viii
LIST OF FIGURES	ix
ABSTRACT	xi
1. INTRODUCTION	1
2. MODEL AND EXPERIMENTS	4
2.1 The Model	4
2.2 Experimental Design	7
2.3 Model Phenomenology	8
3. RESULTS	14
3.1 Model Data Comparisons	14
3.2 Stream Function Analysis	19
3.3 Alenuihaha Channel Flow	23
3.4 Ekman Flow	28
3.5 Hawaiian Islands and Wind	32
3.6 Topographical Influences	35
4. SUMMARY AND CONCLUSIONS	40
APPENDICES	43
APPENDICES	43

A. Symbols	43
REFERENCES	45
BIOGRAPHICAL SKETCH	48

LIST OF TABLES

1	<p>Pacific Ocean simulations north of 20°S. ^a A horizontal grid resolution of 1/16° (1/16° in latitude by 45/512° in longitude) is used for each prognostic variable. Simulations <i>RG1</i> and <i>RG2</i> have 2 layers in the vertical with the lowest layer being infinitely deep and quiescent (commonly referred to as 1.5 layers). Simulations <i>NL1</i> and <i>NL2</i> have 6 layers in the vertical and realistic bottom topography. The 200 <i>m</i> isobath near the shelf break is used as the model boundary in most locations and is the shallowest topography in the model domain. The topography reaches a maximum of 6500 <i>m</i> and is multiplied by 0.8 to confine it to the lowest layer. ^b <i>A</i> is the coefficient of isopycnal eddy viscosity. ^c The seasonal wind forcing is provided by the <i>Hellerman and Rosenstein</i> (1983) (HR) monthly wind stress climatology. ^d Simulation <i>NL1</i> is an extension of an existing 1/16° simulation. Simulation <i>RG1</i> is an extension of a comparable 1/8° simulation. Simulations <i>NL2</i> and <i>RG2</i> are extensions of <i>NL1</i> and <i>RG1</i> respectively with the Hawaiian Islands removed. All simulations are spun-up to near statistical equilibrium. ^e See table 2 for additional information regarding fixed parameters.</p>	8
2	<p>Additional parameters used in simulations <i>NL1</i> and <i>NL2</i>.</p>	9
3	<p>Breakdown and transport of the incoming flow. Transport values are given in Sverdrups (1 <i>Sv</i> = 10⁶<i>m</i>³<i>s</i>⁻¹).</p>	22
4	<p>Transports through transects north (TRN), south (TRS), east (TRE), and west (TRW) of the Hawaiian Islands. Positive (negative) transports represent eastward and northward (westward and southward) flows. The net transport into the boxed region is given by <i>BOX</i> = <i>TRS</i> + <i>TRW</i> - <i>TRE</i> - <i>TRN</i>. Thus, a positive (negative) transport for the boxed region denotes an influx (outflux) of mass over the layer for the boxed region. Transports are given in units of Sverdrups (1 <i>Sv</i> = 10⁶<i>m</i>³<i>s</i>⁻¹).</p>	31

LIST OF FIGURES

1	1/16° model topography of the Hawaiian Islands and major channels. The topography is a modified version of the 1/12° ETOP05 (<i>NOAA</i> 1986) bottom topography.	6
2	Five year mean upper ocean transport stream function (in Sv , where $1 Sv = 10^6 m^3 s^{-1}$) from the 1/16° 6-layer non-linear simulation. Notable differences can be seen from the linear solution including realistic pathways for the Kuroshio and Kuroshio extension as well as an accurate representation of the subarctic front and the North Pacific Current.	10
3	Mean transport stream function (in Sv) for the 1/16° linear reduced gravity simulation.	11
4	NL1 upper layer current vectors superimposed on the mean u velocity (color shading). Note the zonality of the incoming flow, the existence of the North Hawaiian Ridge Current, and the flow reversal in the lee of the islands, the Hawaiian Lee Counter Current. Units are $m s^{-1}$. Contour intervals are given along the right side of the figure. Vector magnitudes are denoted by the arrow on the top right.	14
5	Mean drifter velocities averaged in $1/2^\circ$ bins. Numbers on the right hand side of each bin are the bin number (top) and number of drifter days of observations included in the average (bottom). The principal axes of variance are denoted by the perpendicular lines at the tip of each vector. For the directions indicated, the lengths of each line represent the 90% confidence limits for the mean velocities. Units and scale are shown. Adapted from <i>Bingham</i> (1998).	15
6	Mean flow field derived from 165.7 drifter-years of data taken between 1986 and 1997. The current vectors are estimated on a $0.5^\circ \times 0.5^\circ$ grid taking into account the mean and variance of the currents. Blank areas represent regions where the mean currents are not significantly different from zero at the 90% confidence limit. Adapted from <i>Qiu et al.</i> (1997).	16
7	Five year mean layer (a) 1, (b) 2, (c) 3, and (d) 4 pressure deviation with contour intervals of 0.5, 0.25, 0.125, and $0.125 m^2 s^{-2}$ respectively. Note how the subtropical gyre shifts northward with depth in agreement with <i>Wyrtki</i> (1974).	17
7	(Continued).	18
7	(Continued).	18

8	NL1 upper ocean ($\sim 1 km$) transport stream function (black contours) and RG1 transport stream function (red contours). Contour values are in Sverdrups (Sv), where $1 Sv = 10^6 m^3 s^{-1}$. Contour interval is $0.5 Sv$	20
9	Snapshots of the NL1 layer 1 current field for (a) day 015 and (b) day 228 of model year 180. The snapshots indicate the high levels of variability in the flow as well as the lack of preference for cyclonic or anticyclonic eddies in the vicinity of the NHRC. Clearly, the flow in the region is dominated by nonlinearity and the ubiquitous presence of eddies. Units and scale are shown.	25
10	Four panel figure representing the the unsmoothed <i>Hellerman and Rosenstein</i> (1983) (a) wind stress (vectors in $m s^{-1}$) and wind stress magnitude (contours in Pa), (b) wind stress curl (in $Pa/m \times 10^{-8}$) for the Hawaiian Islands region and the linear transport stream function for the simulations (in Sv) (c) with the islands (RG1) and (d) with the islands removed. Contour intervals are $0.05 Pa$, $2 Pa/m$, $1.0 Sv$, and $1.0 Sv$ for panels (a)-(d) respectively.	33
10	(Continued).	34
11	Five year mean upper ocean transport stream function (black contours, in Sv) superimposed on the layers (a) 1, (b) 6, (c) 2, (d) 3, (e) 4, and (f) 5 five year mean pressure anomaly (red contours, in m). Contour intervals are $0.5 Sv$ for the transport stream function and $0.1 m$, $0.05 m$, $0.025 m$, $0.01 m$, $0.01 m$, and $0.01 m$ for layers 1-6 respectively.	36
11	(Continued).	37
12	Superposition of the five year mean upper ocean transport streamfunction (black contour, in Sv) and the combined layer 1 and 6 pressure anomaly (red contours, in m). Contour intervals are $0.5 Sv$ for the transport streamfunction and $0.1 m$ for the layer 1+6 pressure anomaly.	39

ABSTRACT

Mesoscale features of the time mean flow for the Hawaiian Islands region are examined using a series of four $1/16^\circ$ numerical simulations of the Pacific Ocean north of 20°S . Emphasis is placed on the North Hawaiian Ridge Current (NHRC), which the numerical simulation depicts as a robust surface trapped feature of the mean flow in the central Pacific Ocean. The NHRC manifests from a northern branch of the North Equatorial Current (NEC). Upon impinging on the island of Hawaii, the northern branch of the NEC bifurcates near 20°N separating into two main pathways north and south of Hawaii. In the most realistic simulation, $4.5 Sv$ flows south of Hawaii and joins the southern branch of the NEC, forming the southern boundary of the subtropical gyre. The remaining $6.0 Sv$ forms the $100 km$ wide NHRC. The NHRC begins at the bifurcation point of the northern branch of the NEC, leaks $2.0 Sv$ through the Alenuihaha channel to the lee of the islands, and continues along the Hawaiian Island chain until it reaches Kauai. Past Kauai, the flow veers westward towards the western boundary of the Pacific Ocean basin. The NHRC width scale is consistent with that of an inertial boundary layer. The effects of Ekman pumping/suction, vertical mixing, and the meridional overturning cell on the mean flow are negligible. Averaged over the upper $1 km$, the location of the northern branch of the NEC bifurcation and the mean strength of the NHRC exhibit responses to upper ocean-topographic coupling. Abyssal currents steer upper ocean currents resulting in a northward migration of the bifurcation and enhanced transport north of Hawaii. However, the upper ocean-topographic coupling is not evident in the upper layer current. However, the upper ocean-topographic coupling is not evident in the upper layer cur-

rents. Additionally, comparisons of numerical simulations with the islands and with the islands removed reveals a direct impact of the islands on the regional wind field.

1. INTRODUCTION

The existence and dynamics of a northwestward flowing current along the Hawaiian Islands, the North Hawaiian Ridge Current (NHRC), has been a topic of research since the early 1980's. *Mysak and Magaard* (1983) excited initial interest in the existence of such a boundary current by theorizing the interaction between baroclinic Rossby waves and island ridges could produce narrow boundary currents. *White* (1983) furthered this idea by noting the existence of such a boundary current in XBT data in the vicinity of the Hawaiian Islands. The work of *Mysak and Magaard* (1983) has been extended to include the effects of lateral friction (*Oh and Magaard* 1984) and higher order nonlinear effects (*Graef and Magaard* 1994). The work has been substantiated by its reasonable agreement with observations (*Sun et al.* 1988, *Graef and Magaard* 1994), but *Price et al.* (1994) failed to provide evidence for the existence of the NHRC in AXBT and AVHRR data.

More recently, the NHRC has been found in the long term mean circulation in the region (*Firing* 1996, *Qiu et al.* 1997, *Bingham* 1998), but with high variability and frequent interruptions. However, the dynamics leading up to the existence of the current remain an unanswered question. Aside from the interaction of the ridge with westward propagating Rossby waves (*Mysak and Magaard* 1983, *Oh and Magaard* 1984, *Graef and Magaard* 1994), there are two other hypotheses suggesting the formation of the NHRC (*Qiu et al.* 1997, *Bingham* 1998).

One hypothesis suggests that the NHRC is a western boundary current for the eastern Pacific Ocean subtropical gyre. *Qiu et al.* (1997) have examined the North

Hawaiian Ridge Current (NHRC) using available surface drifter data, a 2.5 layer reduced gravity model of the North Pacific tropical and subtropical oceans, and by applying the "Island Rule" (*Godfrey* 1989). Their work, along with the work of others (*White* 1983, *Talley and DeSzoeko* 1986, *Firing* 1996, *Munch* 1996), provides clear evidence for the existence of the NHRC. The use of the "Island Rule" and the reduced gravity model provides information regarding the leading order dynamics associated with the NHRC. *Qiu et al.* (1997) suggest the NHRC to be an artifact of the mean wind forcing in which the NHRC balances a mismatch between the interior Sverdrup transport and the net southward transport of the gyre. Further, *Qiu et al.* (1997) indicate the improbability of the NHRC owing its presence to westward propagating, baroclinic Rossby waves as suggested by *Mysak and Magaard* (1983).

Another hypothesis purports the NHRC to be a manifestation of a forking of the North Equatorial Current (NEC) (*Bingham* 1998). A series of 227 drifters were examined over a five year period from 1988-1992 to produce a distinct image of the NHRC. *Bingham* (1998) concludes, in agreement with *Firing* (1996), that the Reynolds stress dependent theory of *Mysak and Magaard* (1983) may be an inadequate explanation for the existence of the NHRC. Further, *Bingham* (1998) suggests that although the NHRC exists in the long term mean, it is a highly variable structure with dynamics that are not easily understood.

Clearly, the dynamics behind the formation of the NHRC are still not completely understood. It is the focus of the current research to examine the dynamics of the NHRC by utilizing a high resolution numerical ocean model. Unlike the limited area model used by *Qiu et al.* (1997), the model encompasses the Pacific Ocean basin north of 20°N and includes the barotropic mode. Model results provide evidence suggesting the NHRC to be a manifestation of a northern branch of the NEC. Upon reaching of 20°N and includes the barotropic mode. Model results provide evidence suggesting the NHRC to be a manifestation of a northern branch of the NEC. Upon reaching

Hawaii, the NEC splits into two main pathways with flow traveling south of Hawaii to join the southern branch of the NEC and north of Hawaii forming the NHRC. Time dependent fluctuations of the NHRC are not considered except in relation to the mean flow.

This thesis is organized as follows. Section 2 describes the model and the experiment design. Section 3 discusses the results of the model simulations, including a comparison with observations, a stream function analysis describing the pathways of the flow, a breakdown of the flow through the Alenuihaha Channel and the predominant width scale of the NHRC, the attenuated effects of Ekman pumping/suction, effects of the islands on the wind field, and the influence of topography on the transport of the NHRC. Finally, the conclusions of the study will be summarized in section 4.

2. MODEL AND EXPERIMENTS

2.1 The Model

The Naval Research Laboratory Layered Ocean Model (NLOM) is utilized. The model is a primitive equation layered ocean model that is a descendent of the model by *Hurlburt and Thompson* (1980) with enhanced processing and capability (*Wallcraft* 1991). The vertically integrated equations used in the current version of the NLOM n -layer, finite depth, hydrodynamic model are:

$$\begin{aligned} \frac{\partial \vec{V}_k}{\partial t} + (\nabla \cdot \vec{V}_k + \vec{V}_k \cdot \nabla) \vec{v}_k + \hat{k} \times f \vec{V}_k = -h_k \sum_{l=1}^n G_{kl} \nabla (h_l - H_l) + \quad (1) \\ \frac{(\vec{\tau}_{k-1} - \vec{\tau})}{\rho_0} + \max(0, -\omega_{k-1})v_{k-1} - [\max(0, \omega_{k-1}) + \max(0, -\omega_k)]v_k + \\ \max(0, \omega_k)v_{k+1} + \max(0, -C_M \omega_{k-1})(v_{k-1} - v_k) + A_H \nabla^2 \vec{V}_k \end{aligned}$$

$$\frac{\partial h_k}{\partial t} + \nabla \cdot \vec{V}_k = \omega_k - \omega_{k-1} \quad (2)$$

where, $k = 1 \dots n$ when referring to layers, and $k = 0 \dots n$ when referring to interfaces between layers with $k = 0$ at the surface.

An explanation of the parameters and notation used here is given in the appendix. The model has no-slip and kinematic boundary conditions and is solved on a C-grid (*Messinger and Arakawa* 1976) using a semi-implicit scheme for the finite depth simulations, and an explicit scheme for the reduced gravity experiments. The model includes a free surface and the barotropic mode. A more detailed description of the model is given by *Wallcraft* (1991).

includes a free surface and the barotropic mode. A more detailed description of the model is given by *Wallcraft* (1991).

Although the versions of the model used here are purely hydrodynamic, thermodynamic versions exist (*Metzger et al.* 1992, *Metzger and Hurlburt* 1996). In the hydrodynamic version of the model, thermal forcing and steric anomalies arising from seasonal heating and cooling are neglected. The model does allow the interfaces between model layers to ventilate (isopycnal outcropping).

Isopycnal outcropping occurs when diapycnal mixing is active and the layer thickness (h_k) is less than the layer thickness at which entrainment begins (h_k^+), i.e. when $h_k < h_k^+$. Non-positive layer thickness is prevented by entraining water from a layer below a region of outcropping at a rate necessary to maintain positive layer thickness. In this hydromixing process (*Wallcraft* 1991), momentum and mass are mixed while the density structure remains unchanged.

Mass is conserved within the layers. This is achieved by balancing the accumulation of entrained mass into a region of outcropping by a detrainment of mass elsewhere in the model domain, or via ports in the model boundary. For a more thorough description of the model entrainment/detrainment scheme see *Shriver and Hurlburt* (1997).

The finite depth simulations with realistic bottom topography utilized a modified version of the 1/12° ETOP05 (*NOAA* 1986) bottom topography with extensive corrections to the Hawaiian Islands geometry (figure 1). The ETOP05 data set was interpolated to the model grid and twice smoothed using a 9-point smoother. The smoothing is designed to reduce energy generation at smaller scales which are poorly resolved by the model.

The maximum depth of the model is 6500 m. In the finite depth simulations, seamounts and other rough bottom topography are confined to the lowest layer. As a result, numerical difficulties arising when moving interfaces and sloping topography seamounts and other rough bottom topography are confined to the lowest layer. As a result, numerical difficulties arising when moving interfaces and sloping topography

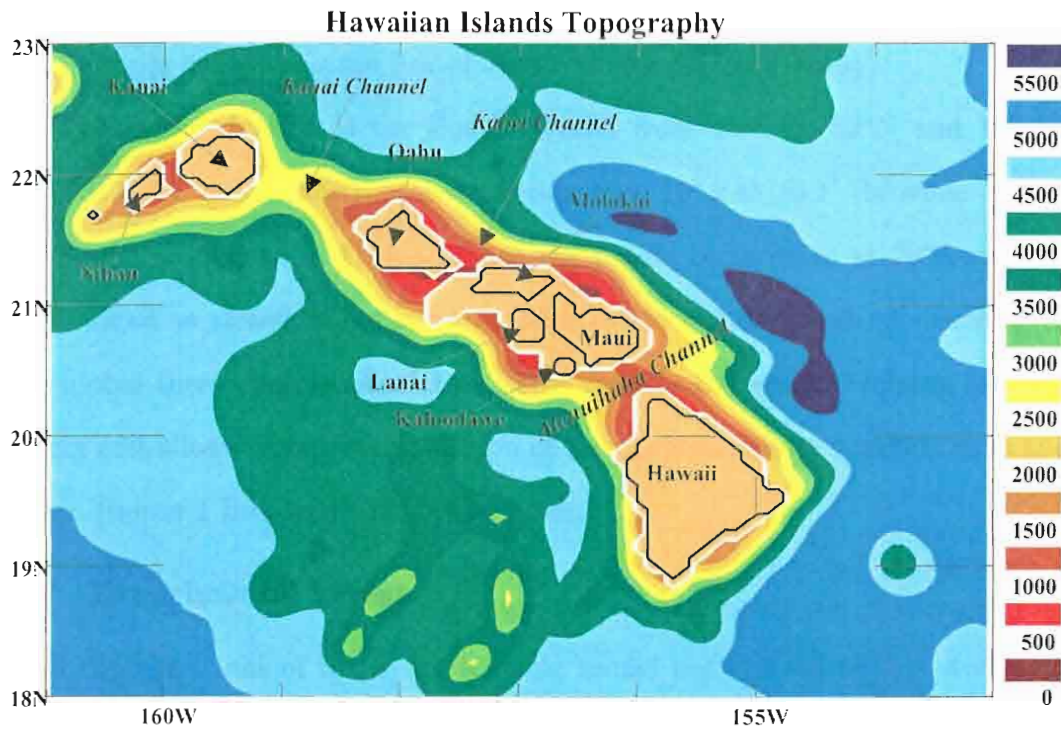


Figure 1: $1/16^\circ$ model topography of the Hawaiian Islands and major channels. The topography is a modified version of the $1/12^\circ$ ETOP05 (NOAA 1986) bottom topography.

intersect are removed (Hurlburt and Thompson 1980). The two primary reasons for including topographic features are to force the lowest layer (abyssal) flow to follow the f/h contours and to regulate baroclinic instability. The confinement of topography to the lowest layer has negligible effect on these. Additionally, flow through straits and shallow sills is constrained to small values below the sill depth.

The model includes realistic coastline geometry with extensive modifications to the Hawaiian Islands compared to ETOP05. The 200 m isobath is used to determine the model boundary and represents the shelf break as well as the minimum depth in the Hawaiian Islands compared to ETOP05. The 200 m isobath is used to determine the model boundary and represents the shelf break as well as the minimum depth in

the model. The only exceptions to this are regions where shallower depths are needed to connect semi-enclosed seas to the Pacific Ocean (e.g. the Tsugaru, Tsushima and Soya Straits connecting the Sea of Japan to the Pacific Ocean).

The model domain is the Pacific Ocean from 20°S to 62°N and 109.125°E to $77.203135^{\circ}\text{W}$ with a horizontal resolution of $1/16^{\circ} \times 45/512^{\circ}$ (latitude \times longitude, hereafter referred to as $1/16^{\circ}$). Since the model boundaries at 20°S and Indonesia are treated as closed, there is no Indonesian throughflow and no contribution from the global thermohaline circulation. This reduces the vertical mixing between lower layers and allows separate calculation of a transport stream function over the upper ocean (upper 1 km) and the abyssal layer.

2.2 Experimental Design

Two configurations of the hydrodynamic model are utilized in this study: 1.5 layer linear reduced gravity and six-layer non-linear finite depth with realistic topography. The linear reduced gravity configuration is used to provide a base case identifying the leading order dynamics associated with the first baroclinic mode, mainly interior *Sverdrup* (1947) flow with *Munk* (1950) style viscous western boundary layers. The six-layer finite depth version then adds dynamics associated with non-linearity, the higher baroclinic modes, the barotropic mode, vertical mixing, and the effects of bottom topography. These dynamics include inertial jets, flow instabilities, topographic steering of currents, isopycnal outcropping, and closed circulations in the vertical.

The only forcing in the simulations used here are the winds. There are no thermal ocean data assimilated in the model except that the density of the model layers are chosen to be consistent with the *Levitus* (1982) oceanic climatology. The simulations were spun up from rest to statistical equilibrium at progressively higher resolution using the *Hellerman and Rosenstein* (1983) (HR) monthly mean wind stress clima-

tology. Summaries of the experiments and model parameters used in this thesis are given in tables 1 and 2.

2.3 Model Phenomenology

A discussion of the model results at the basin-scale is essential to understand the dynamics of the Hawaiian circulation. Most of the basic features of the near surface circulation are present in all of the simulations. Detailed comparisons of the modeled

Table 1: Pacific Ocean simulations north of 20°S . ^a A horizontal grid resolution of $1/16^{\circ}$ ($1/16^{\circ}$ in latitude by $45/512^{\circ}$ in longitude) is used for each prognostic variable. Simulations *RG1* and *RG2* have 2 layers in the vertical with the lowest layer being infinitely deep and quiescent (commonly referred to as 1.5 layers). Simulations *NL1* and *NL2* have 6 layers in the vertical and realistic bottom topography. The 200 m isobath near the shelf break is used as the model boundary in most locations and is the shallowest topography in the model domain. The topography reaches a maximum of 6500 m and is multiplied by 0.8 to confine it to the lowest layer. ^b A is the coefficient of isopycnal eddy viscosity. ^c The seasonal wind forcing is provided by the *Hellerman and Rosenstein* (1983) (HR) monthly wind stress climatology. ^d Simulation *NL1* is an extension of an existing $1/16^{\circ}$ simulation. Simulation *RG1* is an extension of a comparable $1/8^{\circ}$ simulation. Simulations *NL2* and *RG2* are extensions of *NL1* and *RG1* respectively with the Hawaiian Islands removed. All simulations are spun-up to near statistical equilibrium. ^e See table 2 for additional information regarding fixed parameters.

Simulation ^a	A^b $m^2 s^{-1}$	Wind ^c forcing	Years ^d	Comments ^e
RG1	30	Monthly	110 – 125	1.5 Layer, linear, reduced gravity, Winds reduced by a factor of 100.
RG2	30	Monthly	160 – 173	1.5 Layer, linear, reduced gravity, Winds reduced by a factor of 100, Hawaiian Islands removed.
NL1	30	Monthly	178 – 183	6-layer, nonlinear, finite depth.
NL2	30	Monthly	184 – 193	6-layer, nonlinear, finite depth. Hawaiian Islands removed.
NL2	30	Monthly	184 – 193	6-layer, nonlinear, finite depth. Hawaiian Islands removed.

Table 2: Additional parameters used in simulations *NL1* and *NL2*.

Parameter	Definition	Value
C_b	Bottom Drag Coefficient	2×10^{-3}
C_k	kth interfacial stress coefficient	0
g	Gravitational acceleration	9.80 m s^{-1}
h_k^+	Thickness of layer k at which entrainment begins	50 m ($k = 1, 2$) 40 m ($k = 3 - 6$)
h_k^-	Thickness of layer k at which non-compensating detrainment begins	Unused by setting to a large value
$\rho_{k+1} - \rho_k$	Stratification between layers k and $k + 1$	1.97 kg m^{-3} ($k = 1$) 0.91 kg m^{-3} ($k = 2$) 0.35 kg m^{-3} ($k = 3$) 0.21 kg m^{-3} ($k = 4$) 0.38 kg m^{-3} ($k = 5$)
$\sum_{i=1}^k H_i$	Mean depth at base of layer k	135 m ($k = 1$) 320 m ($k = 2$) 550 m ($k = 3$) 800 m ($k = 4$) 1050 m ($k = 5$) bottom ($k = 6$)
$\tilde{\omega}_k$	kth interface reference vertical mixing velocity	0.04 m s^{-1}

basin scale features with altimeter data are given by *Hogan et al. (1992)*, *Hurlburt et al. (1992, 1996)*, *Jacobs et al. (1996)*, and *Mitchell et al. (1996)*. A brief review of the basic large-scale model features will be discussed in the remainder of this section. A more thorough discussion of the Pacific models is given by *Hurlburt et al. (1996)*. Model-data comparisons of the Hawaiian Islands circulation will be discussed later.

The negligible diapycnal mixing of mass between layers 5 and 6 in the model allow for the calculation of a mean transport stream function over the top 5 layers of the 6-layer model. The mean transport stream functions for the $1/16^\circ$ simulations exhibit for the calculation of a mean transport stream function over the top 5 layers of the 6-layer model. The mean transport stream functions for the $1/16^\circ$ simulations exhibit most of the basic, large-scale upper ocean features of the Pacific Ocean circulation.

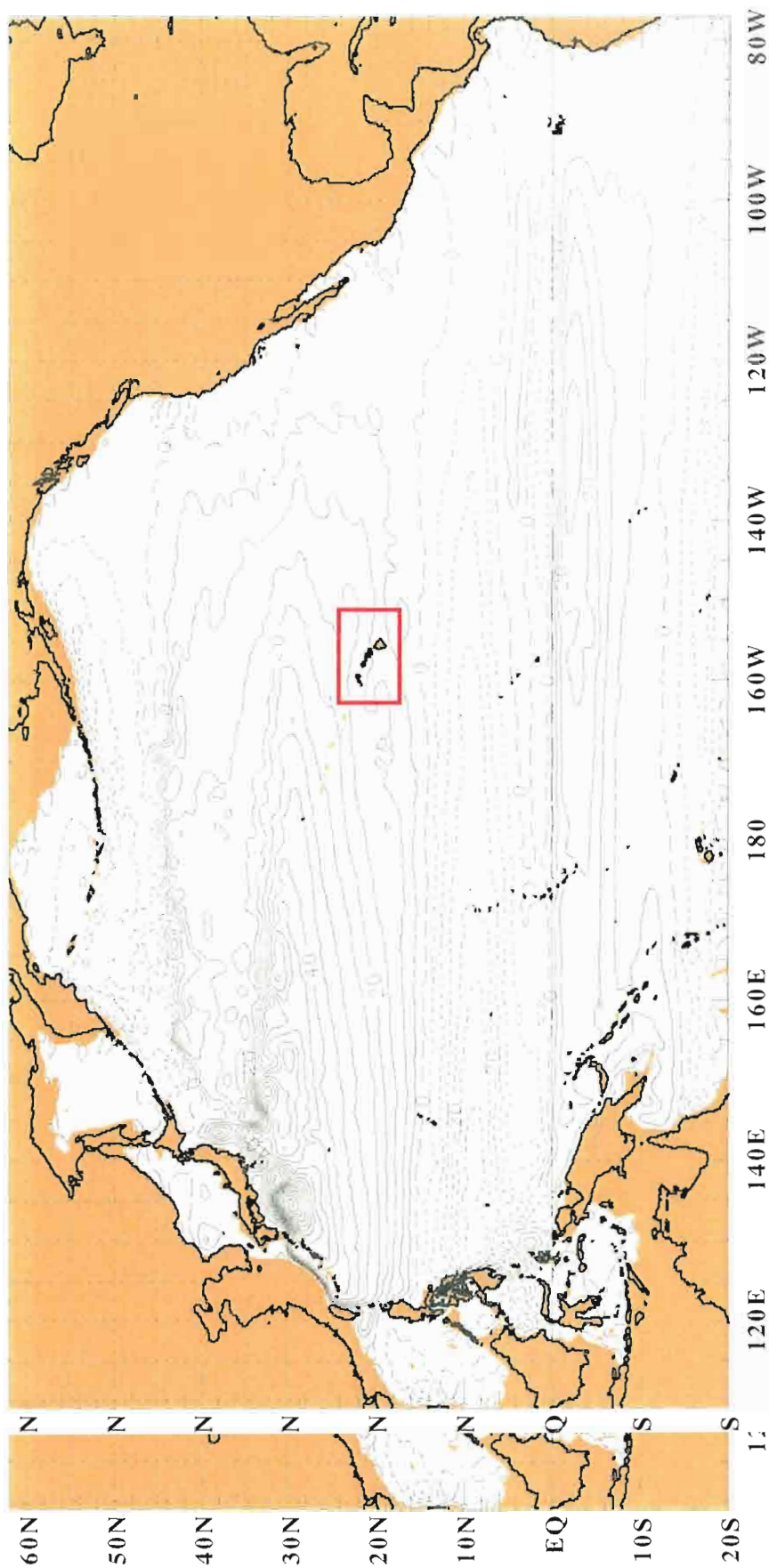


Figure 2: Five year mean upper ocean transport stream function (in Sv , where $1 Sv = 10^6 m^3 s^{-1}$) from the $1/16^\circ$ 6-layer non-linear simulation. Notable differences can be seen from the linear solution including realistic pathways for the Kuroshio and Kuroshio extension as well as an accurate representation of the subarctic front and the North Pacific Current.

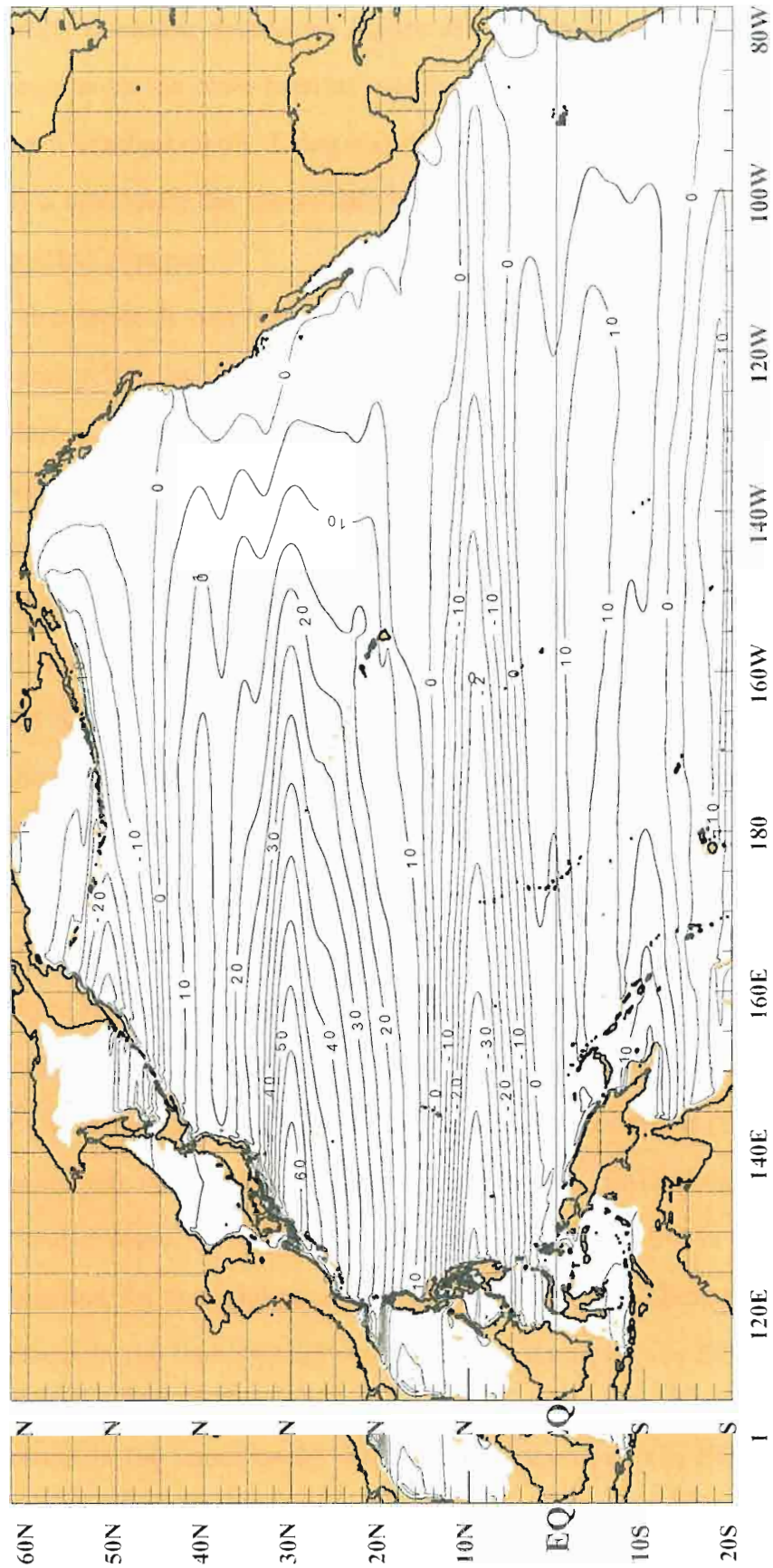


Figure 3: Mean transport stream function (in Sv) for the 1/16° linear reduced gravity simulation.

The strongly nonlinear simulation (figure 2) exhibits more sharply defined currents and fronts due to the more inertial nature of the currents and the large amplitude variations in interface depth. Using realistic geometry and winds, the linear simulation (figure 3) is essentially the numerically calculated linear *Munk* (1950) solution with a *Sverdrup* (1947) interior.

The circulation is dominated by two large features, the cyclonic subpolar gyre and the anticyclonic subtropical gyre. Separating the two, at $\sim 42-45^\circ\text{N}$, is the North Pacific Current/subarctic front. The strongest part of the subtropical gyre is bounded on the north by the Kuroshio Extension at $\sim 34-35^\circ\text{N}$ and on the south by a northern branch of the North Equatorial Current (NEC) at $\sim 10-18^\circ\text{N}$. Part of the northern branch of the NEC is diverted southward at Hawaii, joins the southern branch of the NEC, and extends to the western boundary bifurcating at $\sim 14^\circ\text{N}$ to form the northward Kuroshio and the southward Mindanao Current. The Kuroshio is the western boundary current of the subtropical gyre, while the Mindanao Current is the western boundary current of the northern tropical gyre. The northern tropical gyre is bounded on the north by the NEC and on the south by the North Equatorial Counter Current (NECC) at $\sim 5-7^\circ\text{N}$. Between the NEC and NECC, the center of the northern tropical gyre exhibits a broad region of weak northward flow.

The multi-layered design and vertical mixing capabilities of the 6-layer model allow for the formation of an eastward Equatorial Undercurrent (EUC) (centered on the equator) and westward South Equatorial Current (SEC) (centered at $\sim 2^\circ\text{S}$) in layers 1 and 2 respectively (not shown). However, the EUC is manifested in the stream function for the nonlinear model as eastward flow along the equator which is not present in the linear model which doesn't reproduce the EUC. Further south, at $\sim 7-9^\circ\text{S}$, the eastward South Equatorial Counter Current (SECC) shows up. The is not present in the linear model which doesn't reproduce the EUC. Further south, at $\sim 7-9^\circ\text{S}$, the eastward South Equatorial Counter Current (SECC) shows up. The

SECC is much weaker than the NECC and is confined west of the date line in the nonlinear simulation.

3. RESULTS

3.1 Model Data Comparisons

The numerically calculated flow field (figure 4) compares extremely well with observations. The modeled velocity of the NHRC ($\sim 10\text{-}15 \text{ cm s}^{-1}$) is in close agreement

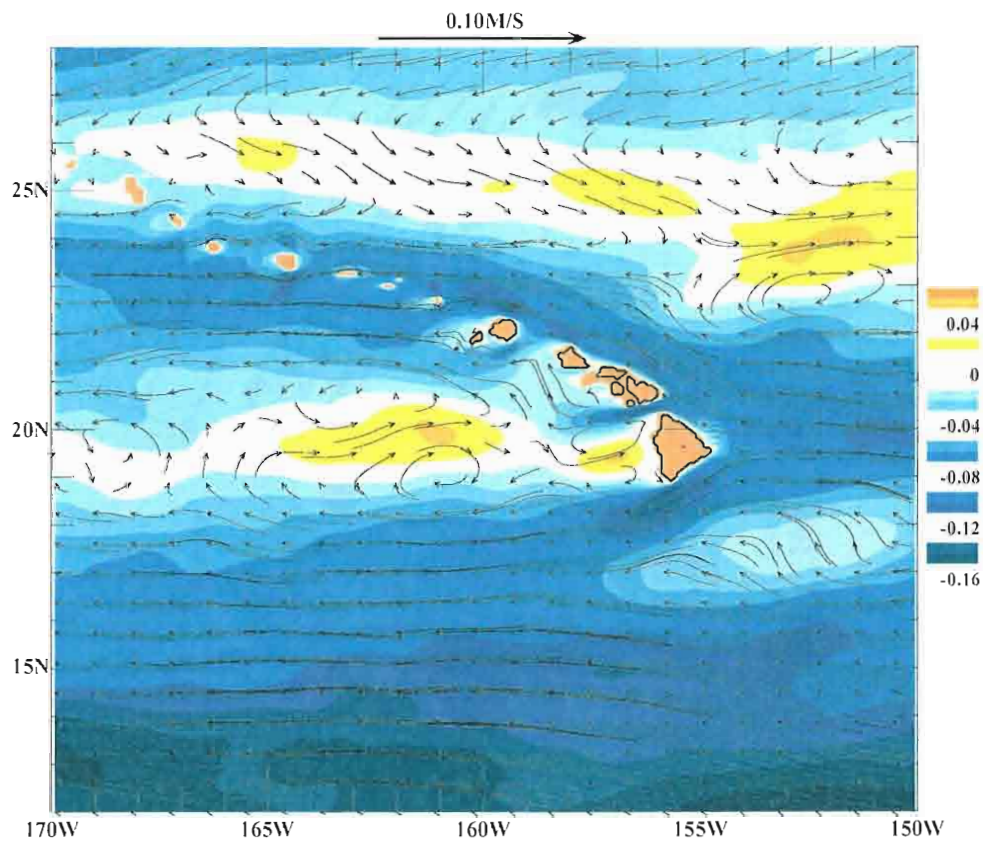


Figure 4: NL1 upper layer current vectors superimposed on the mean u velocity (color shading). Note the zonality of the incoming flow, the existence of the North Hawaiian Ridge Current, and the flow reversal in the lee of the islands, the Hawaiian Lee Counter Current. Units are $m s^{-1}$. Contour intervals are given along the right side of the figure. Vector magnitudes are denoted by the arrow on the top right.

Note the zonality of the incoming flow, the existence of the North Hawaiian Ridge Current, and the flow reversal in the lee of the islands, the Hawaiian Lee Counter Current. Units are $m s^{-1}$. Contour intervals are given along the right side of the figure. Vector magnitudes are denoted by the arrow on the top right.

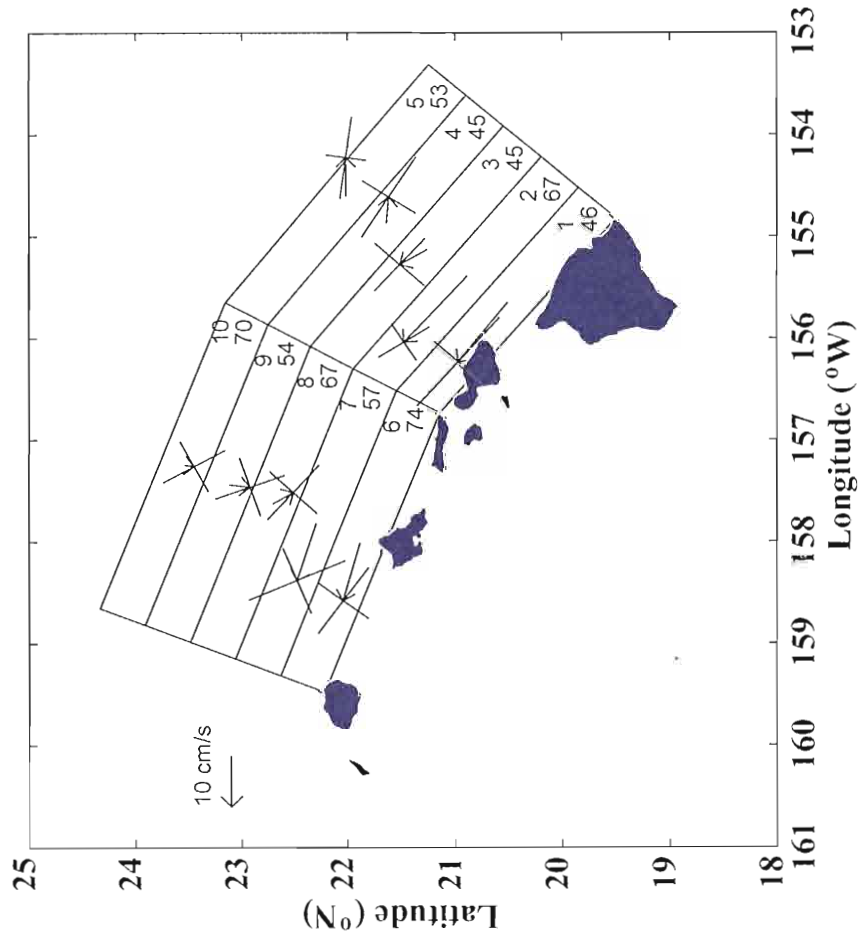


Figure 5: Mean drifter velocities averaged in $1/2^\circ$ bins. Numbers on the right hand side of each bin are the bin number (top) and number of drifter daydrifter days of observations included in the average (bottom). The principal axes of variance are denoted by the perpendicular lines at the tip of each tip of each vector. For the directions indicated, the lengths of each line represent the 90% confidence limits for the mean velocities. Units and scale are shown. Adapted from *Bingham* (1998).

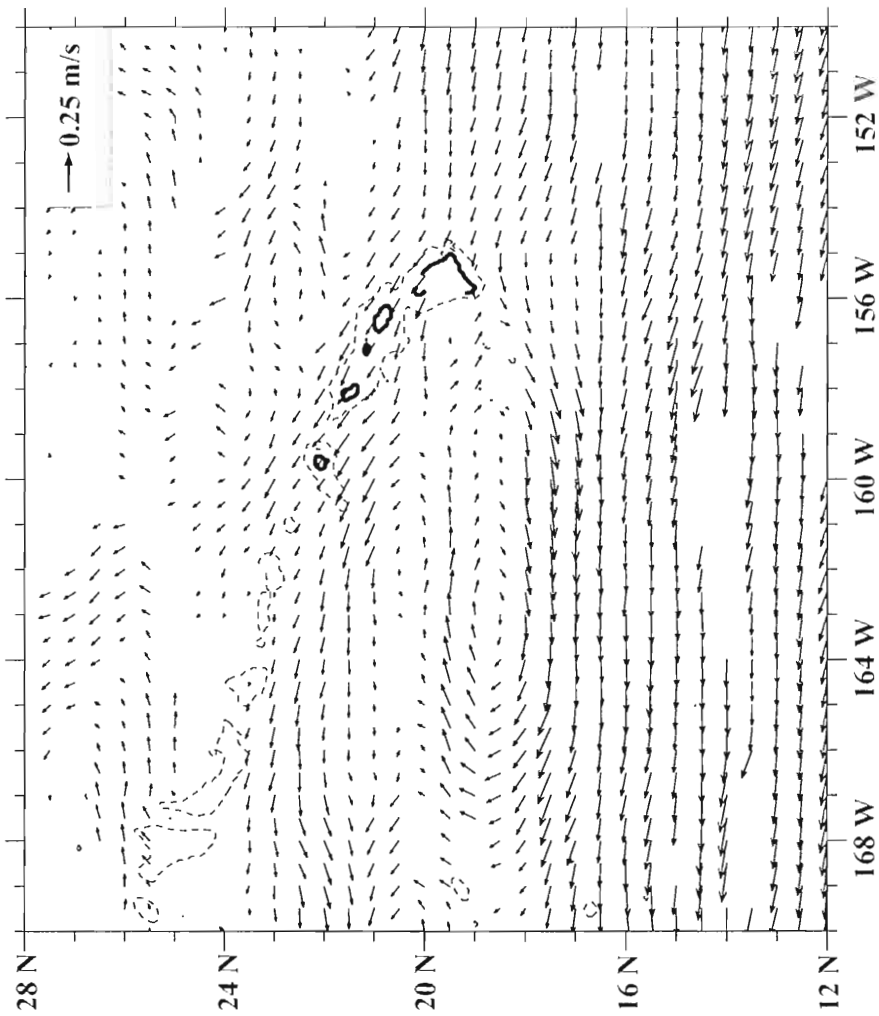


Figure 6: Mean flow field derived from 165.7 drifter-years of data taken between 1986 and 1997. The current vectors are estimated on a $0.5^\circ \times 0.5^\circ$ grid taking into account the mean and variance of the currents. Blank areas represent regions where the mean currents are not significantly different from zero at the 90% confidence limit. Adapted from Qiu *et al.* (1997).

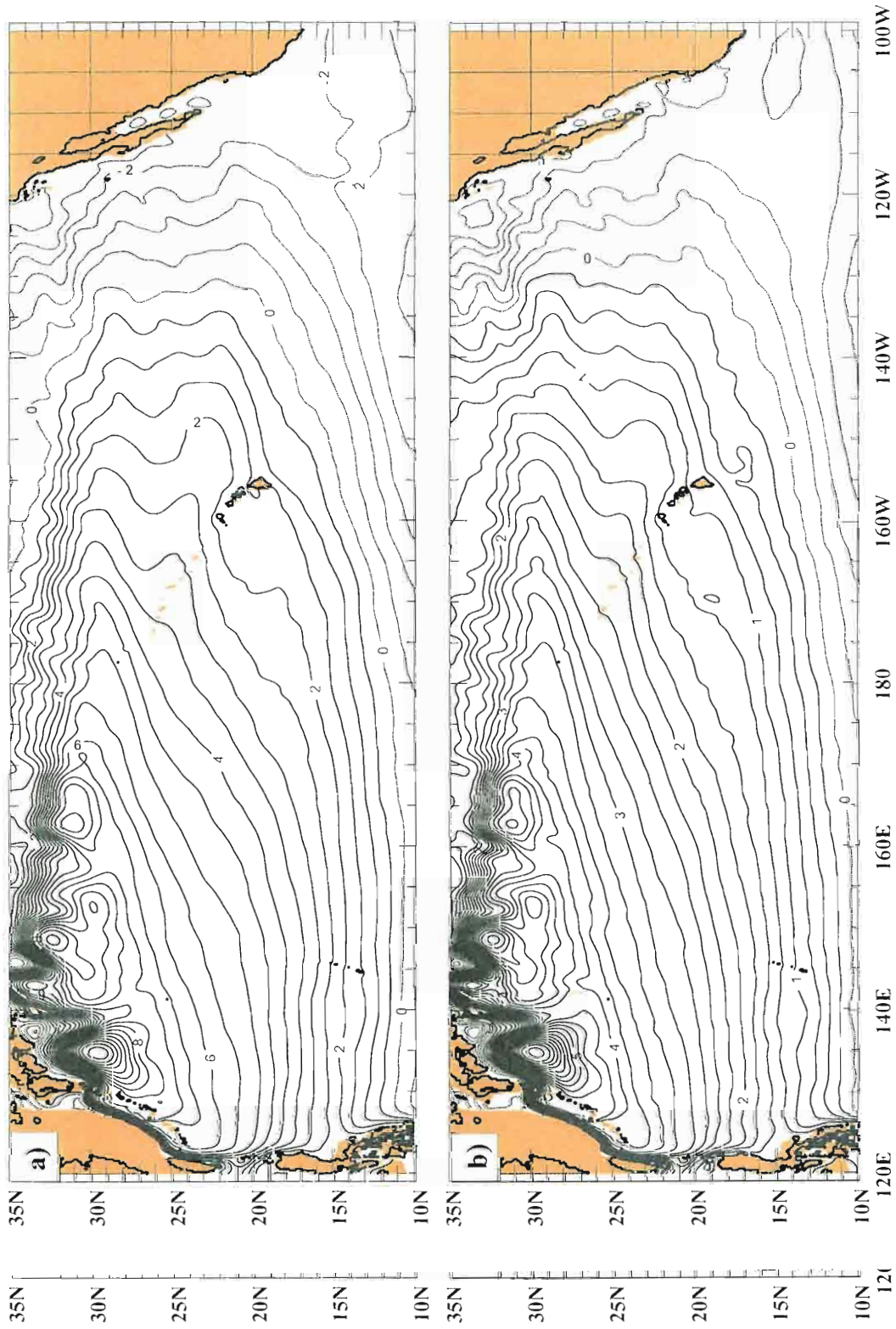


Figure 7: Five year mean layer (a) 1, (b) 2, (c) 3, and (d) 4 pressure deviation with contour intervals of 0.5, 0.25, 0.125, and 0.125 $m^2 s^{-2}$ respectively. Note how the subtropical gyre shifts northward with W_{yrk} (1974)

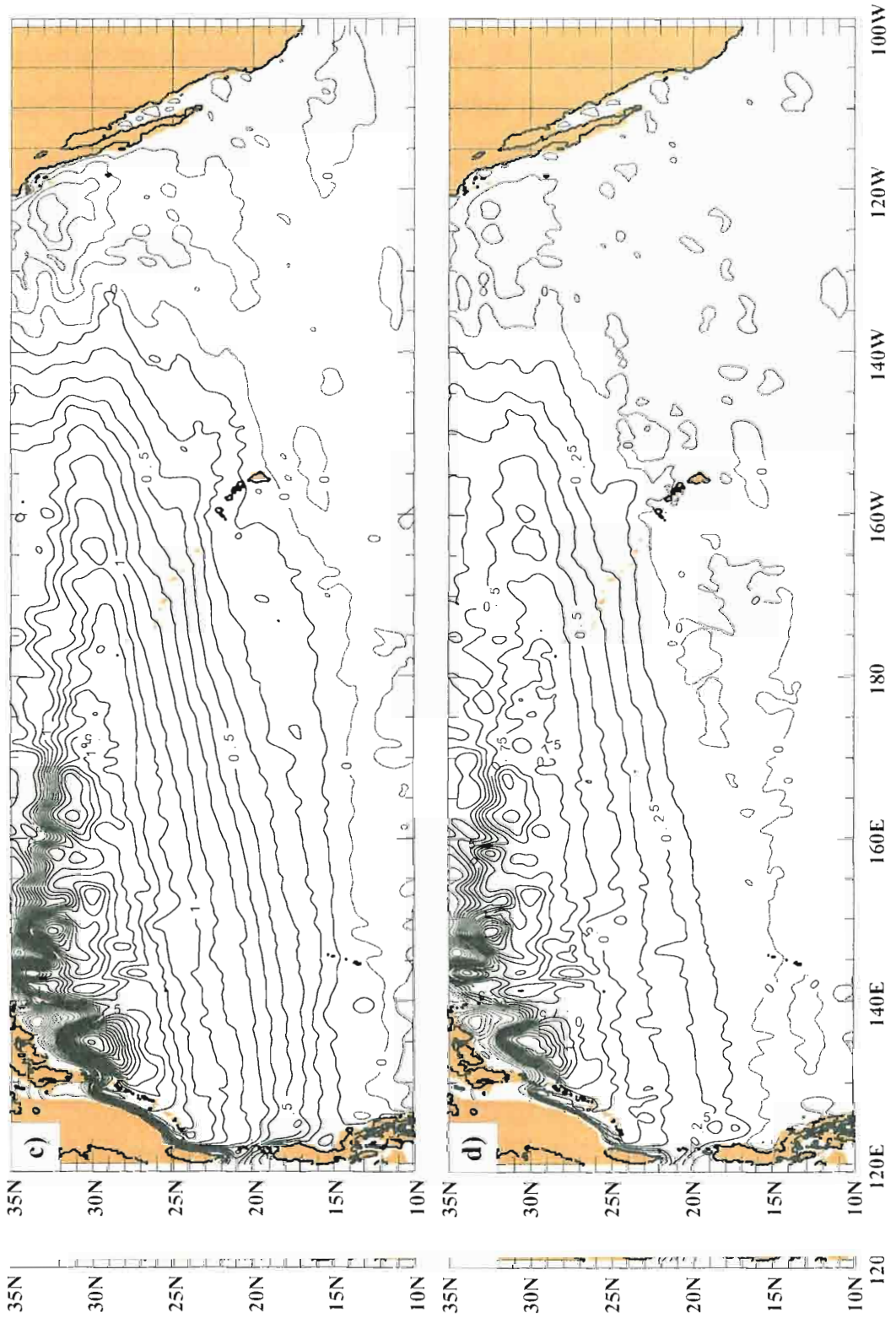


Figure 7: (Continued).

with velocities obtained from both drifters ($\sim 15 \text{ cm s}^{-1}$, figure 5) and from acoustic Doppler current profiler (ADCP) measurements ($\sim 10 \text{ cm s}^{-1}$, *Firing* (1996)). Concurrently, the modeled width of the mean NHRC resembles that obtained from both ADCP (*Firing* 1996) and large scale drifter data (*Qiu et al.* (1997), figure 6). Each produces a mean NHRC with a width of $\sim 100 \text{ km}$. The weakness of the flow field north of the NHRC is evident in the modeled flow as well as the data. Additionally, the model adequately represents the flow reversal seen in the lee of the Hawaiian Islands, the Hawaiian Lee Counter Current (HLCC).

On the basin scale, the model replicates the northward displacement of the subtropical gyre with depth discussed by *Wyrthki* (1974) (figure 7). Thus, the subtropical gyre impacts the Hawaiian Islands in the upper most layers of model, while providing less impact with increasing depth. This produces a unique situation for the flow in the Hawaiian Islands region which has the subtropical gyre dominating the upper ocean flow structure and the bottom topography dominating the flow structure below a few hundred meters depth. This will be discussed in more detail in section 3.6.

3.2 Stream Function Analysis

Cross isopycnal mixing between layers 5 and 6 in the nonlinear, 6-layer, finite depth simulation (hereafter NL1) is negligible. As such, an upper ocean (layers 1-5) transport stream function can be calculated. Comparisons can then be made with the linear reduced gravity simulation (hereafter RG1). The dynamics of the linear model are essentially those of the *Munk* (1950) viscous western boundary layer with a *Sverdrup* (1947) interior, which have been numerically calculated using realistic geometry and wind forcing. Deviations between NL1 and RG1 are explainable by higher order dynamics added in NL1. Stream functions for NL1 and RG1 are presented together in figure 8.

On the regional scale (bottom panel of figure 8) a broad band of westward flow (spanning approximately 18° - 22° N) at 150° W is seen heading towards Hawaii. This flow represents the northern branch of the North Equatorial Current (NEC) stemming

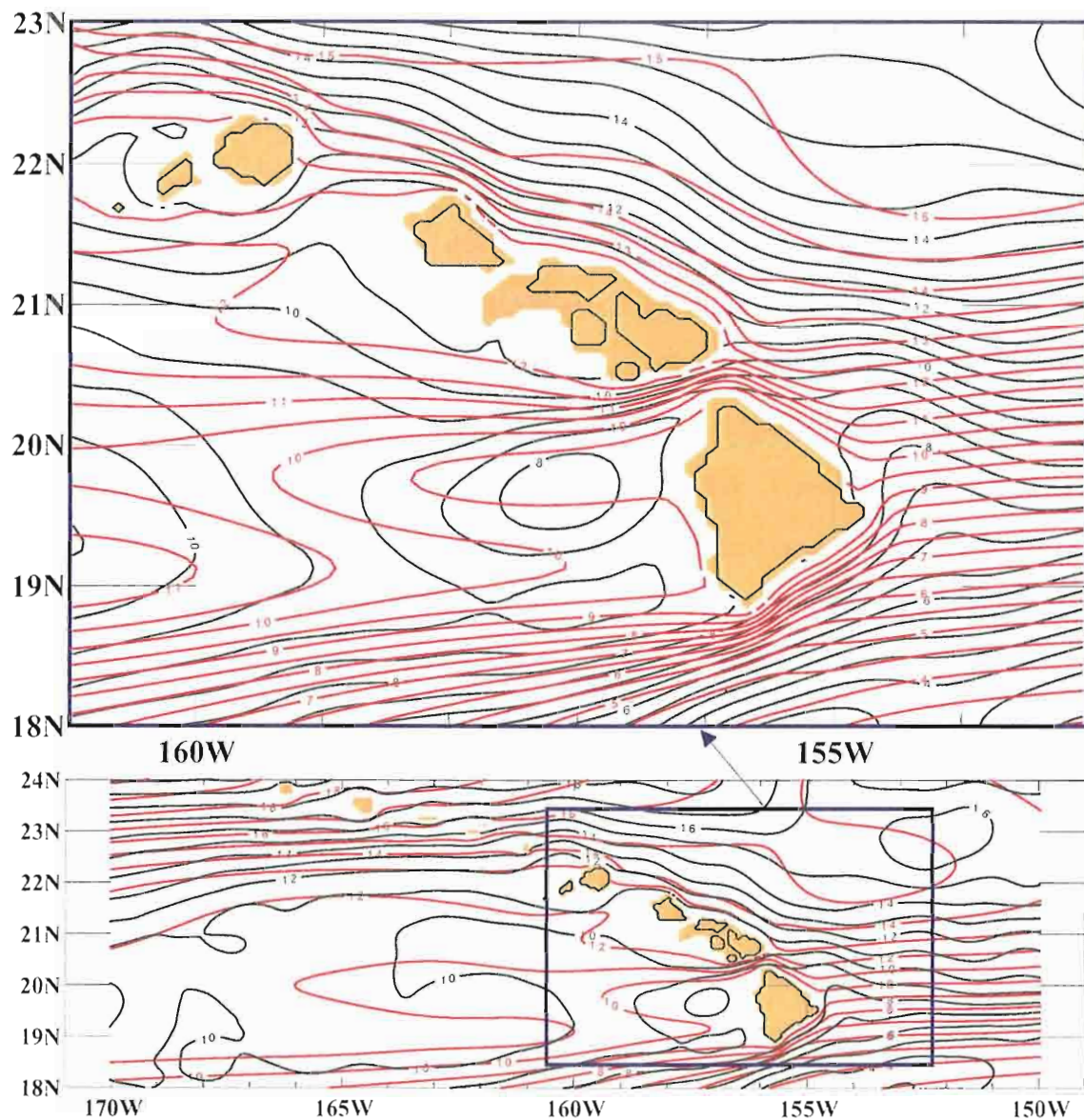


Figure 8: NL1 upper ocean (~ 1 km) transport stream function (black contours) and RG1 transport stream function (red contours). Contour values are in Sverdrups (Sv), where $1 Sv = 10^6 m^3 s^{-1}$. Contour interval is $0.5 Sv$.

Figure 8: NL1 upper ocean (~ 1 km) transport stream function (black contours) and RG1 transport stream function (red contours). Contour values are in Sverdrups (Sv), where $1 Sv = 10^6 m^3 s^{-1}$. Contour interval is $0.5 Sv$.

from the subtropical gyre. Upon impinging on Hawaii, the NEC bifurcates at 20.3°N to form two main pathways, one north of the Hawaiian Islands, the other south of the Hawaiian Islands.

The domain of influence of the incoming flow is taken to range from 18.5°N to 21.5°N . This corresponds to the $4 Sv$ ($4 Sv$) and $14.5 Sv$ ($14.7 Sv$) streamlines for NL1 (RG1). The domain choice was made so that the incoming flow is essentially the same in both the linear and non-linear simulations. A more rigorous examination using boundary layer scaling can be made, but the results are analogous. Even with the convenient domain definition, discrepancies in the pathways of the flow exist. A breakdown of the incoming flow and pathways is given in table 3.

The transport south of Hawaii ($4.5 Sv$) is reduced in NL1 compared with RG1 ($5.5 Sv$). The excess flow is diverted northward by a ridge in the streamline. This featured will be discussed in more detail in section 3.6. Once past the Hawaiian Islands, the transport south of Hawaii continues westward and eventually joins the southern branch of the NEC associated with the boundary between the subtropical and northern tropical gyres (figure 2).

From a dynamical and modeling perspective, the flow branching north at Hawaii has two options, either it can pass through the Alenuihaha Channel (hereafter CHA) between Hawaii and Maui (see figure 1), or it can continue along the island chain as part of the NHRC. This is significant because the transport stream function analysis indicates that some of the flow passes through the Alenuihaha Channel. However, vector arrow plots of the mean current (figure 4) indicate a continuous NHRC beginning at the NEC bifurcation point and continuing past Kauai. As such, the NHRC will be considered to begin at the NEC bifurcation point.

The NHRC is stronger in NL1 ($4.0 Sv$) than in RG1 ($2.5 Sv$). Approximately will be considered to begin at the NEC bifurcation point.

The NHRC is stronger in NL1 ($4.0 Sv$) than in RG1 ($2.5 Sv$). Approximately

66% of this difference is accounted for by more flow passing north of Hawaii and less flowing south of Hawaii at the NEC bifurcation point. The remaining increase is due to a reduction of flow through CHA in NL1 (2.0 Sv) compared with RG1 (2.7 Sv). This allows for an additional 0.7 Sv to continue on with the NHRC towards Kauai. A simple theoretical explanation for the decrease in transport through CHA will be explained in the following section. Additionally, it should be noted that 1.2 Sv (0.8 Sv) passes through the Kaiwi (between Molokai and Oahu) and Kauai (between Oahu and Kauai) channels in NL1 (RG1), with most of the flow passing through the

Table 3: Breakdown and transport of the incoming flow. Transport values are given in Sverdrups ($1 Sv = 10^6 m^3 s^{-1}$).

South of Hawaii (SOH)				
Location	Streamfunction (Sv)		Transport (Sv)	
	Nonlinear	Linear	Nonlinear	Linear
Current Southern Boundary	4.0	4.0	4.5	5.5
South Coast	8.5	9.5		
Alenuihaha Channel (CHA)				
Location	Streamfunction (Sv)		Transport (Sv)	
	Nonlinear	Linear	Nonlinear	Linear
South	8.5	9.5	2.0	2.7
North	10.5	12.2		
North Hawaiian Ridge Current (NHRC) North of CHA				
Location	Streamfunction (Sv)		Transport (Sv)	
	Nonlinear	Linear	Nonlinear	Linear
At Coast	10.5	12.2	4.0	2.5
Off Shore	14.5	14.7		
Total (SOH+CHA+NHRC)			10.5	10.7
Kauai + Kaiwi Channels				
Location	Streamfunction (Sv)		Transport (Sv)	
	Nonlinear	Linear	Nonlinear	Linear
South	10.5	12.2	1.2	0.8
North	11.7	13.0		
Location	Nonlinear	Linear	Nonlinear	Linear
	South	10.5	12.2	1.2
North	11.7	13.0		

latter.

3.3 Alenuihaha Channel Flow

As mentioned in the previous section, the flow through CHA is reduced substantially (by $\sim 26\%$) in NL1 when compared with RG1. At the same time, the NHRC is broadened in NL1 compared to RG1. A simple boundary layer scaling analysis will shed light on the transport discrepancy in CHA while simultaneously discussing the NHRC broadening exhibited in NL1.

NL1 is dominated by an inertial boundary layer scaling, L_I , while RG1 is dominated by a frictional (*Munk* 1950) boundary layer scale, L_M . Both boundary layer scales depend on the β -effect as follows:

$$\begin{aligned} L_M &= \frac{2\pi}{3^{1/2}} \left(\frac{A_H}{\beta_0} \right)^{1/3} \\ L_I &= \left(\frac{V_c}{\beta_0} \right)^{1/2}, \end{aligned} \quad (3)$$

where, V_c and A_H represent the velocity at the core of the current in question, and the coefficient of horizontal viscosity respectively. β_0 represents the variation in coriolis parameter (β -effect) for a given latitude, θ_0 . Taking the mean latitude of the NHRC to be $21.5^\circ N$, $\beta_0 \simeq 2.1 \times 10^{-11} \text{ m}^{-1} \text{ s}^{-1}$.

In order to have a dynamically relevant value of β_0 for our purposes, the angle of the Hawaiian Ridge relative to true north must be taken into account. Following *Hurlburt and Thompson* (1984), β_0 can be divided into:

$$\begin{aligned} \beta_x &= \beta_0 \sin \alpha \\ \beta_y &= \beta_0 \cos \alpha, \end{aligned} \quad (4)$$

where β_x , β_y , and α represent the across ridge component of β_0 , the along ridge component of β_0 , and angle of the ridge counter-clockwise of true north ($90^\circ N$) respectively. β_x , β_y , and α represent the across ridge component of β_0 , the along ridge component of β_0 , and angle of the ridge counter-clockwise of true north ($90^\circ N$) respectively.

Since we are interested in the boundary layer width scale, the appropriate choice of β corresponds to the along ridge component of β , or β_y . Choosing a representative angle of 60° for α , the variation in coriolis becomes, $\beta_y \simeq 1.05 \times 10^{-11} \text{ m}^{-1} \text{ s}^{-1}$. The velocity at the core of the NHRC is roughly 15 cm s^{-1} while the coefficient of horizontal viscosity is $30 \text{ m}^2 \text{ s}^{-1}$, corresponding to boundary layer width scales of $L_I \simeq 120 \text{ km}$ and $L_M \simeq 51 \text{ km}$ respectively. Clearly, the inertial boundary layer width scale is much greater than the frictional boundary layer width scale.

Using the 14.5 Sv (14.25 Sv , not shown) streamfunction from figure 8 as an outer bounds for the boundary layer width for NL1 (RG1) reveals boundary layer scales of $\sim 115 \text{ km}$ and $\sim 50 \text{ km}$ for the nonlinear and linear simulations respectively. The modeled boundary layer width scales and theoretical scales agree extremely well. Like the theory, the inertial boundary layer width associated with the nonlinear model is much greater than the frictional boundary layer width of the linear model. The quantitative agreement between model and theoretical boundary layers width scales suggests a definitive conclusion regarding the spreading of the NHRC, namely, that the width of the NHRC is dictated by the inertial boundary layer scale.

Another possible explanation for the NHRC spreading is the occurrence of preferential eddies, anticyclonic or cyclonic, in the vicinity of the NHRC. Cyclonic (anticyclonic) eddies of the same diameter tend to widen (narrow) the NHRC. However, snapshots of the time dependent flow (two of which are shown in figure 9) do not indicate the preference of either anticyclonic or cyclonic eddies in the vicinity of the NHRC. Thus, it is unlikely that eddy diameters of cyclonic eddies or eddy radii of anticyclonic eddies are setting the width scale of the NHRC.

The snapshots of the time dependent flow (figure 9) also indicate the fact that the NHRC is not a spatially and temporally continuously defined current. The amplitude

The snapshots of the time dependent flow (figure 9) also indicate the fact that the NHRC is not a spatially and temporally continuously defined current. The amplitude

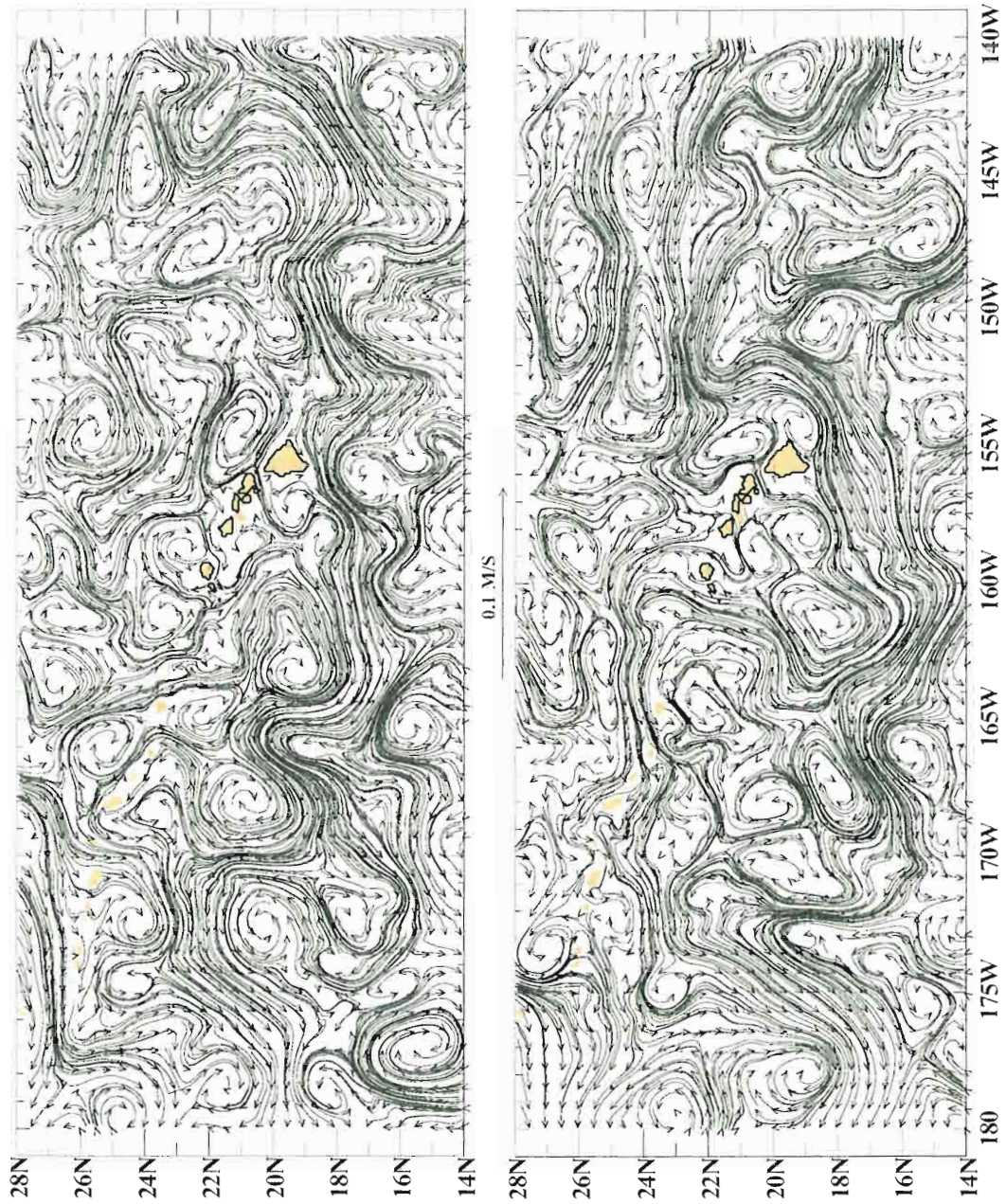


Figure 9: Snapshots of the NL1 layer 1 current field for (a) day 015 and (b) day 228 of model year 180. The snapshots indicate the high levels of variability in the flow as well as the lack of preference for cyclonic or anticyclonic eddies in the vicinity of the NHRC. Clearly, the flow in the region is dominated by nonlinearity and the ubiquitous presence of eddies. Units and scale are shown.

and variability of the flow field is on the order of the NHRC magnitude. As such, the NHRC may be interrupted or even reversed at times. Thus, nonlinear interactions in the flow field must be accounted for when discussing the dynamics of the NHRC.

The boundary layer scaling analysis can also be used to explain why the flow through CHA is reduced in NL1. The Alenuihaha Channel is $\sim 37 \text{ km}$ wide in the model. Offshore of the island of Hawaii, all of the contours contained within 37 km of the coastline flow through the channel, capturing virtually all of the NHRC transport south of the northern edge of the channel. In NL1, the incoming stream function is nearly parallel to CHA and the stream function contours within the latitude range of the channel pass through it. However, because the NHRC is greater than 2 times wider in NL1, the transport stream function contours are farther apart than in RG1 and as a result, the transport through CHA is reduced and the NHRC transport to the north is increased in NL1.

This is a very simple explanation for the reduction in flow through CHA. In order to better understand the phenomenon, it is necessary to examine (1) the influence of the viscous and inertial westward bending space scales for free jets with a meridional component separating from a coastline, and (2) the effect of any quadratic hydraulic flow arising from a pressure head in the channel.

For a northward or southward flowing current, there will be a space scale on which the flow will begin to bend westward. This westward bending space scale depends on the boundary layer scale set by the model. A westward current will have a minimum westward bending space scale, while an eastward flowing current will have a maximum bending space scale. The westward bending space scales for NL1 (denoted as b_I) and RG1 (b_M) can be approximated by:

RG1 (b_M) can be approximated by:

$$b_I = L_I (1 + \cos \theta_I) \quad (5)$$

$$b_M = L_M (1 + \cos \theta_I), \quad (6)$$

where, L_I and L_M are the inertial and frictional boundary layer scales as previously defined, and θ_I is the inflow angle (measured from the positive x -axis) of the core of the current at the southernmost latitude of the Alenuihaha Channel, in this case $\theta_I \sim 150^\circ$. Numerical verification of the westward bending space scale can be found in *Hurlburt et al.* (1996) (their figure 2(e)). Using the values of L_I and L_M determined above, the maximum penetration of the NHRC in the process of westward bending after separating from the northeast coast of Hawaii is $b_I \sim 16 \text{ km}$ and $b_M \sim 7 \text{ km}$ for the inertial and frictional boundary layer scales respectively.

Thus, upon reaching CHA, the flow will begin to bend westward and the core of the current will only reach the maximum northward penetration distance before being completely diverted westward. This may be crucial in RG1 since some of the flow passes along the coast of Hawaii before reaching CHA. However, the more zonal approach of the NHRC to CHA in NL1 shows that the westward bending scale is not a significant issue in determining the flow through the channel in NL1.

However, we need to consider the contributions from the linear geostrophic flow and the quadratic hydraulic flow through CHA. *Metzger and Hurlburt* (1996) adapted the theory of *Mattsson* (1995) to examine the relative contributions of the two flow regimes to the flow through a strait in a 1.5-layer reduced gravity model. The specifics of the calculation are left to the conscientious reader. Here, it suffices to say that given the characteristic scales for CHA and the flow through it, the contribution from linear geostrophic flow is at least an order of magnitude greater than that from the quadratic hydraulic flow and thus, the transport through CHA is not significantly reduced by a hydraulically induced pressure head.

The magnitude of flow through CHA in NL1 is dependent upon the fact that a

ridge in the streamline diverts the flow northward. This disallows the possibility of the upper ocean (depth averaged) flow being affected by the westward bending space scale. Instead, the reduction in transport through CHA (and subsequent NHRC enhancement) crucially depends on the width of the NHRC in relation to the width of CHA and the location and direction of the inflow in relation to the orientation of CHA. The location and direction of the inflow are governed by the topography as will be discussed in section 3.6.

Finally, the boundary layer analysis of flow through CHA can also be used to investigate the increase in NHRC magnitude from RG1 to NL1 in a very simple fashion. An examination of table 3 sheds some light on the subject. The mass transport budget indicates that $1 Sv$ extra transport is diverted north of Hawaii while simultaneously the flow through CHA is reduced by $0.7 Sv$ in NL1. The difference, $1.7 Sv$, matches the difference in NHRC strength between NL1 and RG1, $1.5 Sv$, to within 12%.

3.4 Ekman Flow

The direct wind forcing is limited to the topmost layer. However, the wind stress can influence the subsurface flow through a pressure gradient set up by the Ekman pumping or suction at the base of the upper layer. The geographical location of the Hawaiian Islands suggests that Ekman pumping associated with negative wind stress curl over the subtropical gyre may produce a substantial contribution to the overall flow. Therefore, it is necessary to examine the relative contribution from Ekman pumping/suction to the long term mean circulation (in this case, five years).

The most useful tool for understanding the contribution from Ekman pumping/suction for the long term mean is the vorticity equation. The vorticity equation

ing/suction for the long term mean is the vorticity equation. The vorticity equation

for the reduced gravity model is:

$$\frac{\partial \zeta}{\partial t} + \vec{V} \cdot \nabla \zeta + (\zeta + f) \left(\frac{\partial u}{\partial x} + \frac{\partial v}{\partial y} \right) + \beta v = \frac{1}{\rho} \nabla \times \left(\frac{\tau_s - \tau_i}{h} \right) + A_H \nabla^2 \zeta, \quad (7)$$

where, $\zeta = \frac{\partial u}{\partial x} - \frac{\partial v}{\partial y}$ is the relative vorticity, τ_s the surface stress, τ_i the interfacial stress, and the remaining terms are as previously defined.

The vorticity equation represents the balance of vorticity sources and sinks (right hand side of equation (7)) with the local time rate of change in relative vorticity (first term, left hand side), the relative vorticity advection (second term, left hand side), the stretching/compression of the fluid column (third term, left hand side), the planetary vorticity advection (fourth term, left hand side), frictional effects in the vertical including the wind forcing (first term, right hand side), and the lateral dissipation by viscous friction (second term, right hand side).

The vortex stretching/compression response to changes in the wind stress curl is known as Ekman pumping/suction. We can rewrite the vortex stretching term using the continuity equation,

$$\frac{\partial u}{\partial x} + \frac{\partial v}{\partial y} = -\frac{1}{h} \frac{dh}{dt}. \quad (8)$$

Substituting equation (8) into equation (7), the vorticity equation becomes

$$\frac{\partial \zeta}{\partial t} + \vec{V} \cdot \nabla \zeta - (\zeta + f) \frac{1}{h} \frac{dh}{dt} + \beta v = \frac{1}{\rho} \nabla \times \left(\frac{\tau_s - \tau_i}{h} \right) + A_H \nabla^2 \zeta. \quad (9)$$

Viewing the vorticity equation in this form illuminates the relationship between Ekman pumping/suction and the wind stress curl, namely, that for a positive (negative) wind stress curl, the layer thickness will decrease (increase).

During the spin-up process, changes in the wind and interfacial stresses produce fluctuations in the layer thickness (as small perturbations in a linear model). Rossby

During the spin-up process, changes in the wind and interfacial stresses produce fluctuations in the layer thickness (as small perturbations in a linear model). Rossby waves and Kelvin waves assist in the adjustment to a quasi-steady state as described

by *Cane* (1979). In a linear model, the end result is interior *Sverdrup* (1947) flow with a *Munk* (1950) viscous western boundary layer represented by:

$$\beta V = \frac{1}{\rho} \nabla \times \left(\frac{\tau_s - \tau_i}{h} \right) + A_H \nabla^2 \zeta. \quad (10)$$

Similar analysis holds true for the nonlinear, multi-layer results, except that as the circulation reaches equilibrium, the *Munk* (1950) viscous western boundary layer is replaced with an inertial boundary layer. For the long term mean, this is represented by:

$$\vec{V} \cdot \nabla \zeta - (\zeta + f) \frac{\vec{V}}{h} \cdot \nabla h + \beta V = \frac{1}{\rho} \nabla \times \left(\frac{\tau_s - \tau_i}{h} \right). \quad (11)$$

Unlike the linear case which utilizes lateral diffusion, the advection of relative vorticity plays a crucial role in maintaining the vorticity balance in the nonlinear model. Thus, Ekman pumping/suction and Rossby waves are an adjustment process leading to interior *Sverdrup* (1947) flow with an inertial (viscous) western boundary layer in NL1 (RG1).

There are two main areas where strong diapycnal mixing occurs in the model, the subpolar gyre and along the equator. The subpolar gyre exhibits strong diapycnal mixing as a result of intense Ekman suction occurring in the gyre. The equator, on the other hand, exhibits strong diapycnal mixing as a consequence of the thermocline tilting along the equator. In both cases, the diapycnal mixing transfers mass from lower layers to upper layers.

Conservation of volume within a layer in the model requires the diapycnal mixing occurring in the subpolar gyre and along the equator to be compensated by downward diapycnal mixing elsewhere in the model domain. In some regions, this diapycnal mixing can lead to large changes in the modeled circulation. Therefore, it is important to examine the contribution to the flow resulting from diapycnal mixing for the Hawaiian

Islands region. This is accomplished by examining the net transport of mass into/out of each layer.

The transports through each transect and their sums are given in table 4. The transports are calculated by summing the U (V) transports across north-south (east-west) transects for the eastern (TRE), southern (TRS), western (TRW), and northern (TRN) sides of the box and multiplying by the length of the side. The transports and sums are calculated so that the transports are positive northward and eastward. The transports are then summed so that the total transport into the box for each layer is obtained.

A small amount of mass is transferred from layer 1 to layer 2 indicating that the region participates in the meridional overturning circulation associated with diapycnal mixing in the subpolar gyre and the equatorial region. Upward diapycnal mixing in the subpolar gyre and along the equator results in an equatorward (poleward) flow towards the subtropical gyre from the subpolar gyre (equator). The subtropical gyre then compensates for the excess mass by mixing it to the layers below. Some of this

Table 4: Transports through transects north (TRN), south (TRS), east (TRE), and west (TRW) of the Hawaiian Islands. Positive (negative) transports represent eastward and northward (westward and southward) flows. The net transport into the boxed region is given by $BOX = TRS + TRW - TRE - TRN$. Thus, a positive (negative) transport for the boxed region denotes an influx (outflux) of mass over the layer for the boxed region. Transports are given in units of Sverdrups ($1 Sv = 10^6 m^3 s^{-1}$).

Transect	Layer 1	Layer 2	Layer 3	Layer 4	Layer 5	Layer 6	Total
TRE	-5.38	-4.96	-1.26	-0.42	-0.01	0.48	-11.55
TRS	-1.69	-2.45	-0.44	-0.11	0.10	4.40	-0.19
TRW	-1.95	-2.50	-0.79	-0.29	-0.09	-5.62	-11.25
TRN	1.60	0.22	0.04	0.01	-0.01	-1.75	0.11
BOX	0.14	-0.21	-0.01	0.01	0.03	0.05	0.00
TRW	-1.95	-2.50	-0.79	-0.29	-0.09	-5.62	-11.25
TRN	1.60	0.22	0.04	0.01	-0.01	-1.75	0.11
BOX	0.14	-0.21	-0.01	0.01	0.03	0.05	0.00

mixing occurs over the Hawaiian Islands region. The net effect of the mixing is to increase (decrease) the upper layer (layer 2) thickness in the vicinity of the Hawaiian Islands. The effect is not large enough to greatly affect the circulation, but is a noteworthy addition to the modeled dynamics of the circulation in the region.

For both the nonlinear and linear cases, Ekman pumping/suction plays a critical role in defining the dynamics of the basin scale circulation. On the short time scales, Ekman pumping/suction provides a great deal of communication between the surface and lower layers via diapycnal mixing. In the absence of layer outcropping in the region, Ekman pumping/suction plays no direct role in the mean layer averaged circulation, although it could be included in the long term mean by adding a thin top layer ($\sim 40 m$) with a fixed depth (*Cane* 1979). Therefore, the contributions to NHRC dynamics arising from Ekman pumping/suction are important in establishing the layer thicknesses and interface locations on the basin scale, and in time varying flow, but are not a significant contributor to the dynamics of the mean NHRC.

3.5 Hawaiian Islands and Wind

An interesting side note gleaned from this research involves the effect the islands have on the wind field. The wind stress curl and magnitude for the Hawaiian Islands region are presented in figure 10. The results of RG1 are compared with results from a tandem simulation with the Hawaiian Islands removed (RG2). The transport stream functions (figure 10 (c) and (d)) indicate the incoming flow is identical in the two simulations. However, downstream there are distinct differences as would be expected. The net effect of the islands is to produce a large gradient in the wind stress curl field leading to spreading of the flow in the direct lee of the islands and bunching north and south of the islands downstream. The effect is probably underestimated by the *Hellerman and Rosenstein* (1983) wind set but even so produces a clearly visible

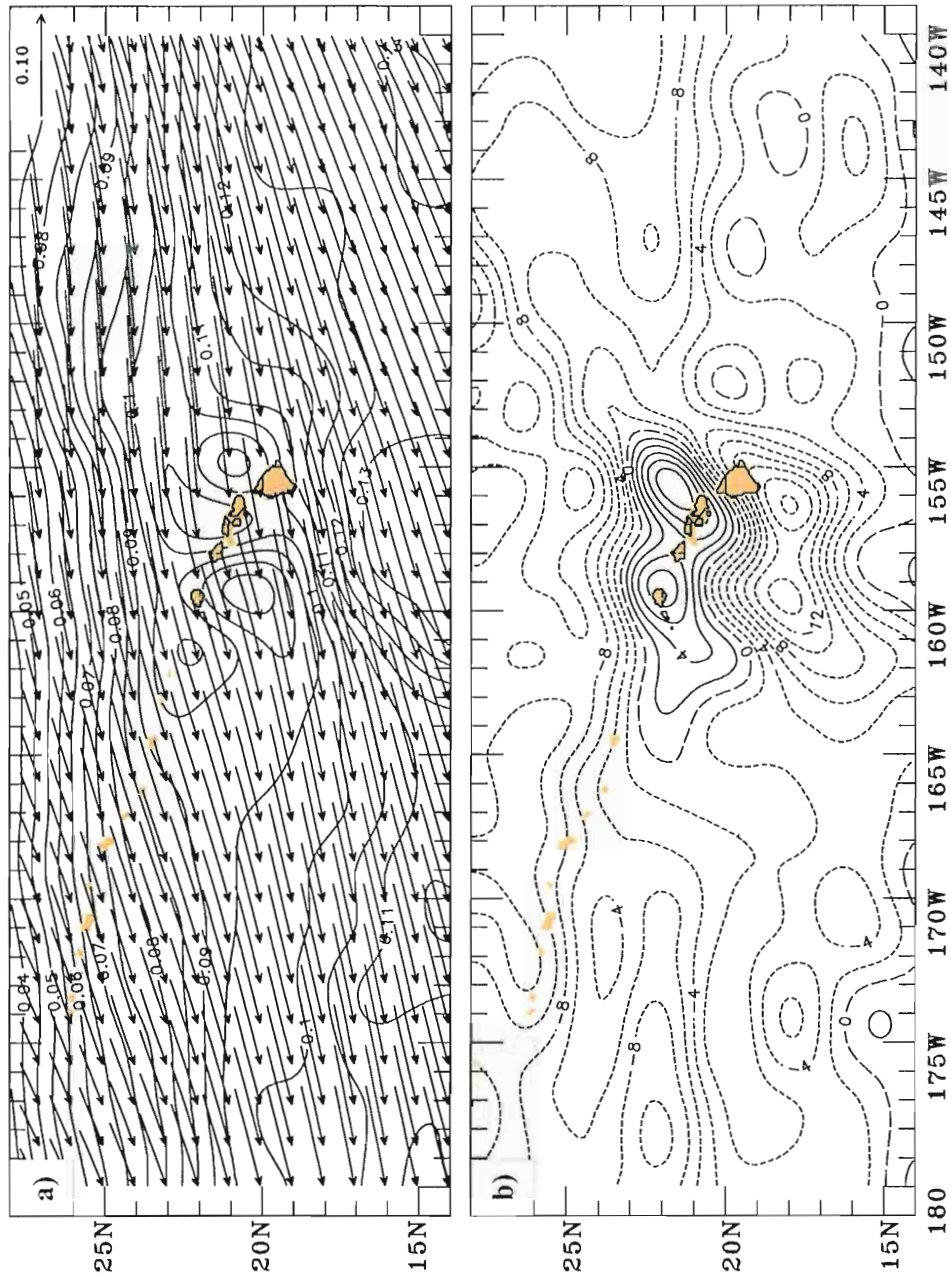


Figure 10: Four panel figure representing the the unsmoothed *Hellerman and Rosenstein* (1983) (a) wind stress (vectors in $m s^{-1}$) and wind stress and stress magnitude (contours in Pa), (b) wind stress curl (in $Pa/m \times 10^{-8}$) for the Hawaiian Islands region and the linear transport stream function for the simulations (in Sv) (c) with the islands (RG1) and (d) with the islands removed. Contour intervals are $0.05 Pa$, $2 Pa/m$, $1.05a/m$, $1.05v$, and $1.05v$ for panels (a)-(d) respectively.

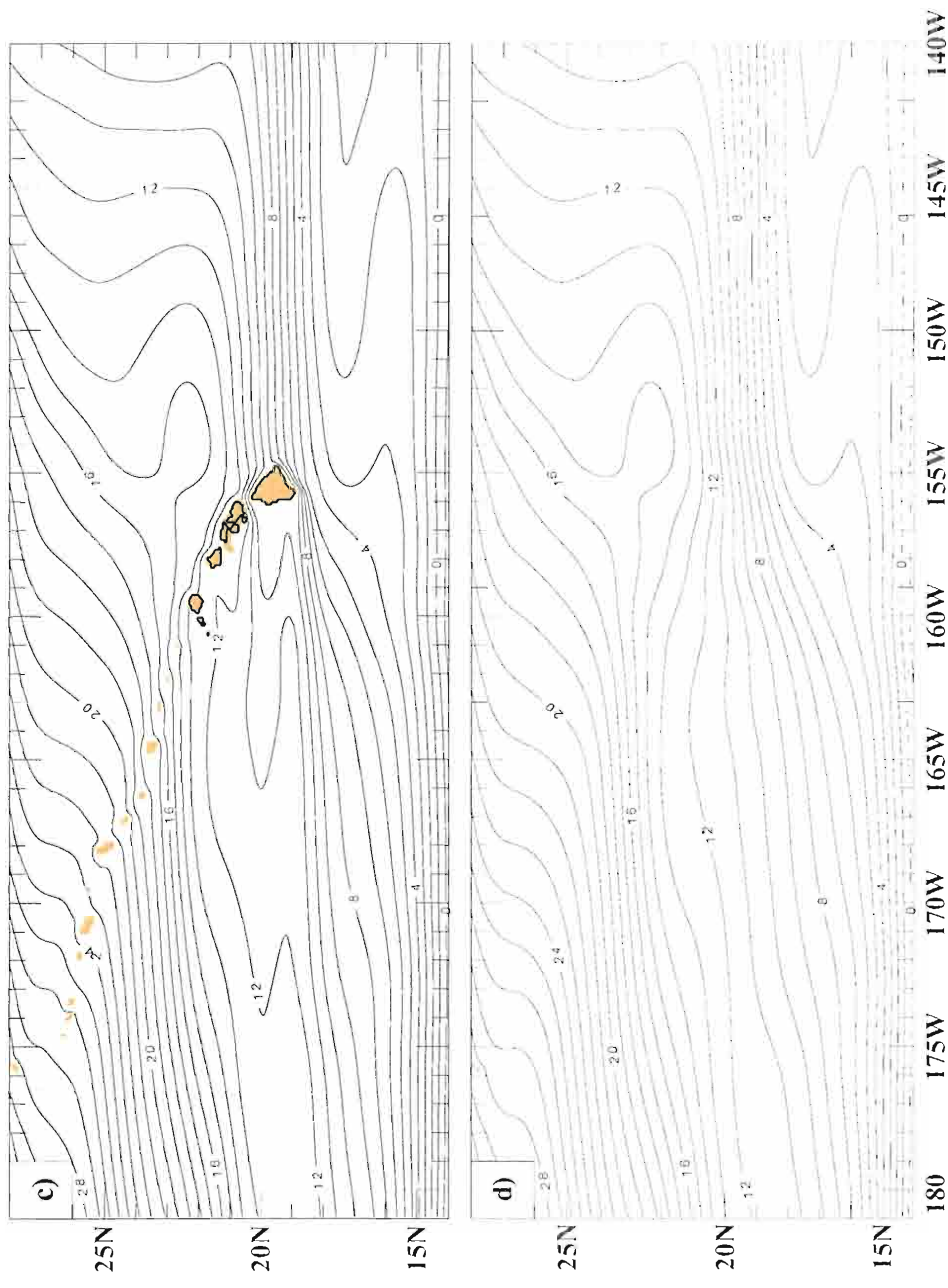


Figure 10: (Continued).

impact on the flow in RG2.

3.6 Topographical Influences

As mentioned previously, a ridge in the incoming westward flow diverts flow northward while reducing the flow traveling south of Hawaii. An examination of the flow at depth (figure 11(b)) does not indicate that the ridge and subsequent displacement of flow are directly related to topographic steering via the abyssal layer flow. Simultaneously, the upper layer current field (figure 4) and zonality of the flow in RG1 (not shown) suggest the ridge is not a wind driven feature. The question is, then, why is the ridge evident in the upper ocean streamfunction and not in the upper layer flow?

The distribution of anomalous pressure with depth provides some insight to this question. As is expected, the upper layer pressure anomaly (figure 11(a)) represents the mean sea surface height signature. This coincides with the zonal flow structure provided by the layer 1 currents (figure 4). Similarly, the abyssal layer pressure anomaly (figure 11(b)) indicates the correlation with the abyssal layer flow which is forced to follow the f/h contours of the bottom topography. However, the mid depth pressure anomalies (figure 11(c)-(f)) reveal the influence of the abyssal layer flow on the upper ocean circulation.

The influence begins as an intense low pressure anomaly residing over a topographical depression, resulting in a cyclonic vortex in the abyssal layer. The pressure anomaly is carried into the upper ocean at mid-depth before succumbing to the wind driven flow in layer 1. Interestingly, the pressure anomaly is shifted southwestward with decreasing depth. The vertically integrated effect is to first accelerate the flow northward via the topographically steered abyssal layer flow, and then steer it southward, producing the ridge. Therefore, although the barotropic signal is not evident in the upper layer current field, the upper ocean recognizes the influence of the topography, producing the ridge. Therefore, although the barotropic signal is not evident in the upper layer current field, the upper ocean recognizes the influence of the topo-

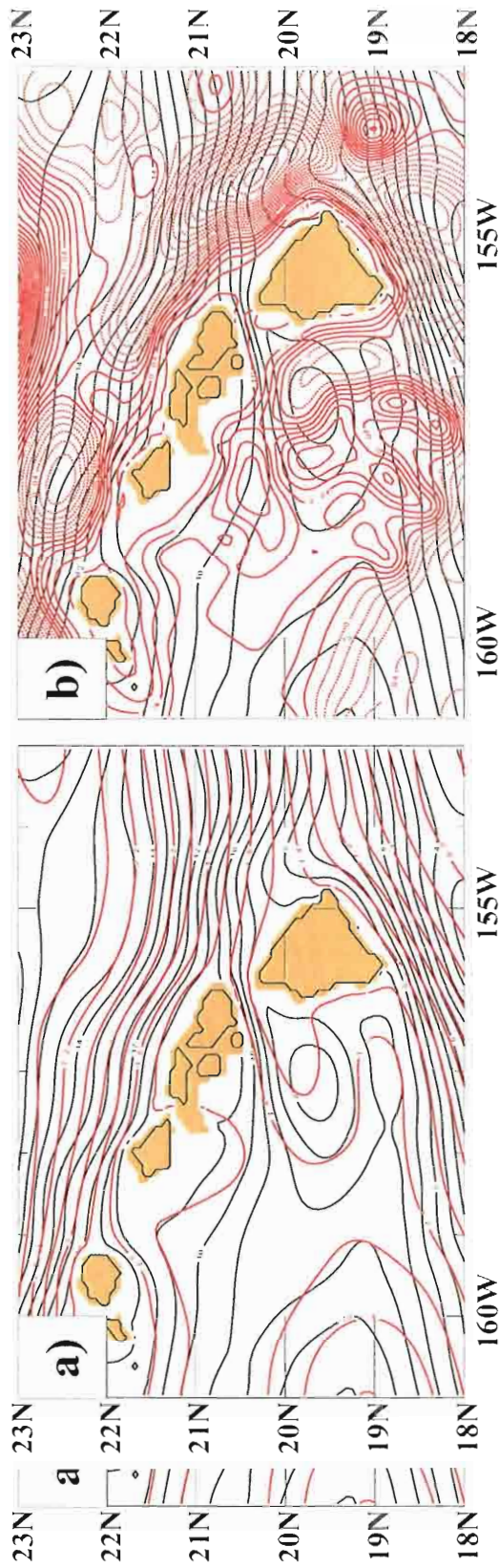


Figure 11: Five year mean upper ocean transport stream function (black contours, in Sv) superimposed on the layers (a) 1, (b) 6, (c) 2, (d) 3, (e) 4, (f) 5 five year mean pressure anomaly (red contours, in m). Contour intervals are $0.5 Sv$ for the transport stream function and $0.1 m$, $0.1 m$, $0.05 m$, $0.025 m$, $0.01 m$, $0.01 m$, and $0.01 m$ for layers 1-6 respectively.

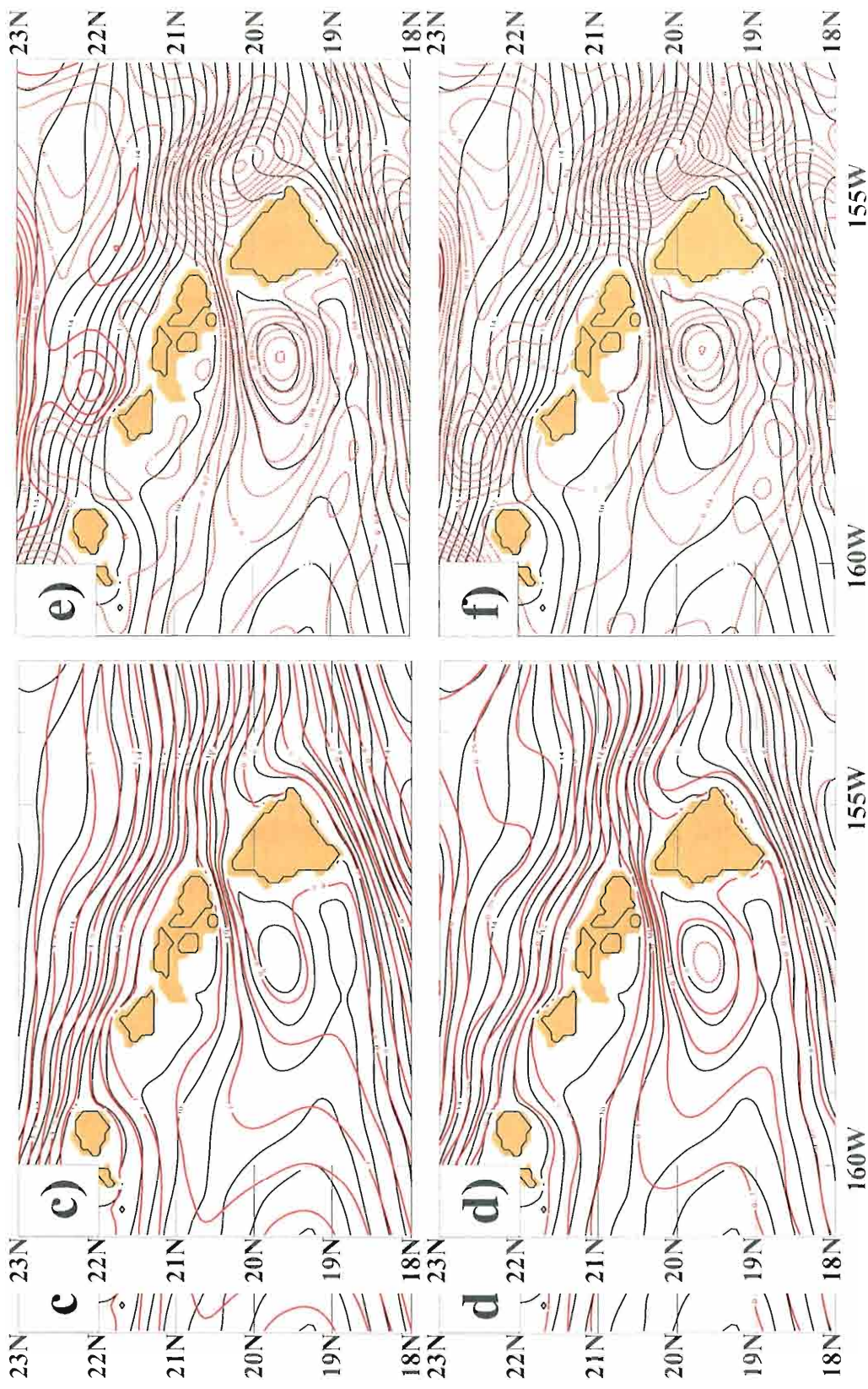


Figure 11: (Continued).

graphically steered abyssal layer flow in the mean transport.

Following *Hurlburt and Thompson* (1980, 1982, 1984) the continuity equation can be examined to show how the upper ocean currents can be steered by the abyssal layer flow. In a 2-layer model it can be shown that:

$$\vec{V}_{1g} \cdot \nabla h_1 = \vec{V}_{2g} \cdot \nabla h_1, \quad (12)$$

where \vec{V}_{kg} is the geostrophic velocity of layer k . The left hand side of (12) represents the contribution to the advection term in the continuity equation (equation (2)) brought about by geostrophy for layer 1. Additionally, the geostrophic balance for the internal mode in a 2-layer model is given by:

$$\hat{k} \times f(\vec{V}_{1g} - \vec{V}_{2g}) = g' \nabla h_1, \quad (13)$$

where $g' = g(\rho_2 - \rho_1)/\rho_0$. In a typical 2-layer ocean model, $|\vec{V}_{1g}| \gg |\vec{V}_{2g}|$. Therefore, (13) indicates that ∇h_1 is a good approximation to \vec{V}_{1g} . For the given circumstances, this indicates that lower layer currents can advect gradients in the upper layer thickness, which in turn steers the upper ocean currents. In the case of a transport streamfunction, the direction of the streamline is not altered, but the curvature is.

The above discussion holds true for a 2-layer model. *Hurlburt et al.* (1996) extended the theory of *Hurlburt and Thompson* (1980, 1982, 1984) to the multilayer case. They show that although the theory is degenerate in multilayer (> 2) models, the steering effect remains in situations in which the first baroclinic and the barotropic modes dominate.

The strength of the first baroclinic mode and the barotropic mode is obtained by adding the pressure anomalies from layers 1 and 6 together and superimposing the results on the upper ocean (layer 1-5) transport stream function (figure 12). The adding the pressure anomalies from layers 1 and 6 together and superimposing the results on the upper ocean (layer 1-5) transport stream function (figure 12). The results show the close agreement between the transport stream function and the first

baroclinic and the barotropic mode. Therefore, it is apparent that the first baroclinic and the barotropic mode are in fact dominating the flow in the Hawaiian Islands region and that there is strong upper ocean-topographic coupling involved in the dynamics of the NHRC.

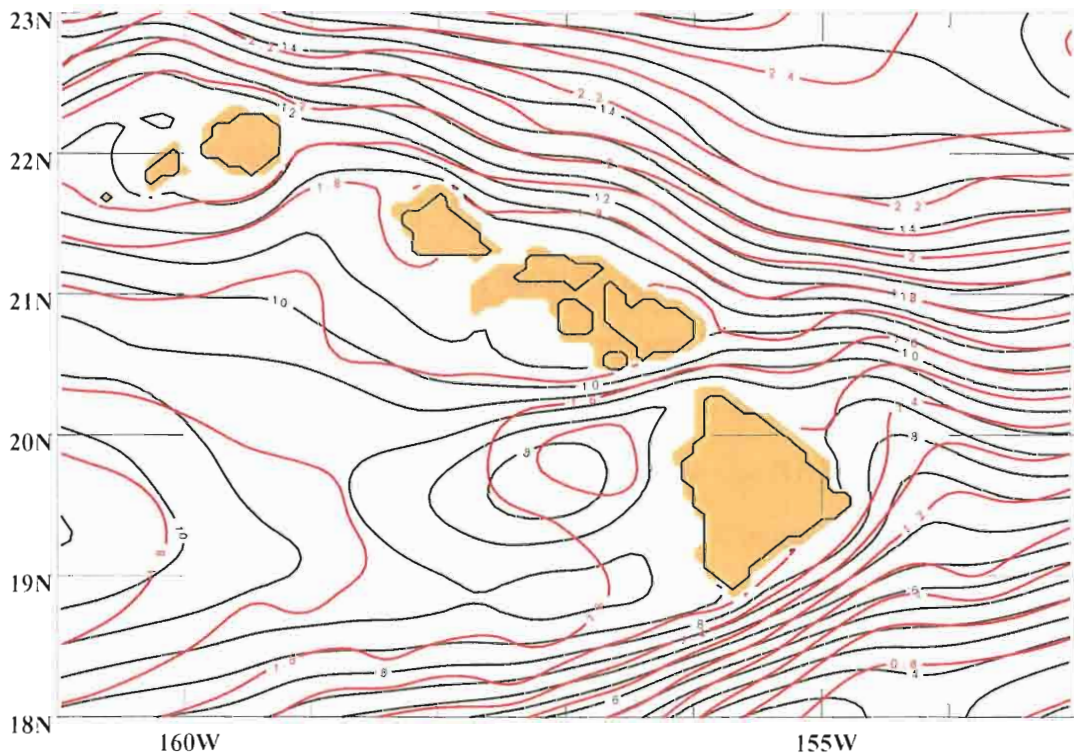


Figure 12: Superposition of the five year mean upper ocean transport streamfunction (black contour, in Sv) and the combined layer 1 and 6 pressure anomaly (red contours, in m). Contour intervals are $0.5 Sv$ for the transport streamfunction and $0.1 m$ for the layer 1+6 pressure anomaly.

Figure 12: Superposition of the five year mean upper ocean transport streamfunction (black contour, in Sv) and the combined layer 1 and 6 pressure anomaly (red contours, in m). Contour intervals are $0.5 Sv$ for the transport streamfunction and $0.1 m$ for the layer 1+6 pressure anomaly.

4. SUMMARY AND CONCLUSIONS

The dynamics of the North Hawaiian Ridge Current (NHRC) have been examined using high resolution ($1/16^\circ$ in latitude) results from the Naval Research Laboratory Layered Ocean Model (NLOM). The ability of the model to reproduce observational data helps make it a useful tool to investigate the dynamics. Nonlinear six-layer finite depth results were compared with linear reduced gravity results in an effort to dissect the fundamental processes necessary for the formation of the NHRC and to understand the dynamics of the flow. Time dependent variations in the NHRC were not considered aside from their impact on the five year mean.

Two seasonally robust branches of the North Equatorial Current (NEC) are found to exist in the modeled circulation. The southern branch, associated with the northern tropical gyre, spans the basin between $10\text{-}15^\circ\text{N}$ latitude. The northern branch stems from the subtropical gyre to feed ~ 10.5 Sverdrups (Sv) of flow into the Hawaiian region. Once the NEC reaches Hawaii, it bifurcates at $\sim 20^\circ\text{N}$ into two main pathways with $4.5 Sv$ going south of Hawaii and $6.0 Sv$ forming the NHRC. Of the northward flowing NHRC, $2.0 Sv$ leaks through the Alenuihaha Channel between Hawaii and Maui. The remaining $4.0 Sv$ continues on with the NHRC until reaching Kauai where it veers westward and continues to the western boundary of the Pacific Ocean. The flow traveling south of Hawaii eventually joins the southern branch of the NEC and continues to the western boundary.

The NHRC is not found to be a western boundary current in the sense that it continues to the western boundary.

The NHRC is not found to be a western boundary current in the sense that it does not close any contours to the east except as a modification of the wind field. The

NHRC is a surface trapped feature existing in the top 3 layers which are dominated by the subtropical gyre. Below layer 3, the subtropical gyre is almost entirely north of the Hawaiian Islands allowing topographical influences to dominate which cause the flow to reverse with depth.

Individual snapshots of the flow indicate the ubiquitous eddy nature and extreme nonlinearity of the mesoscale oceanic flow of the region. As such, the NHRC can not be thought of as a purely linear feature dominating the overall flow structure. The NHRC is a highly variable feature that exists as a robust low latitude current in the five year mean, but may not exist at any given time, even with climatological forcing.

Nonlinear results indicate a reduction in flow through the Alenuihaha Channel. Simultaneously, there is a broadening of the NHRC. Both are attributed to nonlinearity associated with a change from a viscous (*Munk* 1950) boundary layer width in the linear model to an inertial boundary layer width in the nonlinear model. The Alenuihaha Channel is wide enough to accommodate all of the incoming flow in the linear model, while it is too narrow to accommodate all of the nonlinear flow.

The effects of Ekman pumping/suction and vertical mixing were examined through a mass transport budget. The absence of isopycnal outcropping in the region indicates that vertical mixing does not provide a substantial impact on the flow. The effects of Ekman pumping/suction are negligible in the five year mean.

Topographical influences in the approach current are exhibited in the transport of the NHRC. A strong low pressure anomaly in the abyssal layer east of Hawaii produces a ridge in the incoming flow resulting in increased transport north of Hawaii. Although the upper ocean recognizes the influence of the topographically steered abyssal layer flow, it is not evident in the flow field of the topmost layer.

A side note obtained through the study shows the effect of the Hawaiian Islands flow, it is not evident in the flow field of the topmost layer.

A side note obtained through the study shows the effect of the Hawaiian Islands

on the wind field and the effects of the atmospheric perturbations on the oceanic response. The effects were examined by comparing two linear reduced gravity simulations, one with the Hawaiian Islands included, the other with the islands removed. The islands produce strong gradients in the wind stress curl field that are probably underestimated by the *Hellerman and Rosenstein* (1983) winds, but which produce a visible impact on the flow in the simulation without the islands, including spreading of the NEC downstream of the location where the islands were removed.

Appendix A. Symbols

Symbol	Definition
a	radius of the Earth (6371 km);
A_H	coefficient of isopycnal eddy viscosity;
C_b	coefficient of bottom friction;
C_k	coefficient of interfacial friction;
C_M	coefficient of additional interfacial friction associated with entrainment;
$D(\phi, \theta)$	ocean depth at rest;
f	coriolis parameter;
g	acceleration due to gravity;
$G_{kl} = g$	$l \geq k$;
$G_{kl} = g - g \frac{\rho_k - \rho_l}{\rho_0}$	$l < k$;
h_k	kth layer thickness;
h_k^+	kth layer thickness at which entrainment starts;
h_k^-	kth layer thickness at which detrainment starts;
H_k	kth layer thickness at rest;
$H_n = D(\phi, \theta) - \sum_{l=1}^{n-1} H_l$	
$\hat{i}, \hat{j}, \hat{k}$	unit vectors positive eastward, northward, and upward respectively;
t	time;
\vec{v}_k	kth layer velocity;
\vec{V}_k	$h_k \vec{v}_k$;
θ	latitude;
\vec{V}_k	$h_k \vec{v}_k$;
θ	latitude;

- ϕ longitude;
 ρ_k kth layer density (constant for space and time);
 ρ_0 reference density (constant);
 $\vec{\tau}_w$ wind stress;
 $\vec{\tau}_k = \vec{\tau}_w \quad k = 0$;
 $\vec{\tau}_k = C_k \rho_0 |\vec{v}_k - v_{k+1}| (\vec{v}_k - v_{k+1}) \quad k = 1 \dots n - 1$;
 $\vec{\tau}_k = C_b \rho_0 |\vec{v}_n| \vec{v}_n \quad k = n$;
 $\omega_k = 0 \quad k = 0, n$;
 $\omega_k = \omega_k^+ - \omega_k^- - \Omega_k \dot{\omega}_k \quad k = 1 \dots n - 1$;
 $\omega_k^+ = \tilde{\omega}_k \left[\frac{\max(0, h_k^+ - h_k)}{h_k^+} \right]^2$;
 $\omega_k^- = \tilde{\omega}_k \left[\frac{\max(0, h_k - h_k^-)}{h_k^-} \right]^2$;
 $\hat{\omega}_k = \frac{\int \int (\omega_k^+ - \omega_k^-)}{\int \int \Omega_k}$;
 $\tilde{\omega}_k$ kth interface reference diapycnal mixing velocity;
 $\Omega_k(\phi, \theta)$ kth interface weighting factor for mass conservation.

REFERENCES

- Bingham, F. M., Evidence for the existence of a North Hawaiian Ridge Current, *Journal of Physical Oceanography*, *in press*, 1998.
- Cane, M. A., The response of an equatorial ocean to simple wind stress patterns: I. Model formulation and analytic results, *Journal of Marine Research*, *37*, (2), 233–252, 1979.
- Firing, E., Currents observed north of Oahu during the first five years of HOT, *Deep Sea Research*, *43*, 281–303, 1996.
- Godfrey, J. S., A Sverdrup model of the depth-integrated flow for the World Ocean allowing for island circulations, *Geophysical and astrophysical fluid dynamics*, *45*, 89–112, 1989.
- Graef, F., and L. Magaard, Reflection of nonlinear baroclinic Rossby waves and the driving of secondary mean flows, *Journal of Physical Oceanography*, *24*, 1867–1894, 1994.
- Hellerman, S., and M. Rosenstein, Normal monthly wind stress over the World Ocean with error estimates, *Journal of Physical Oceanography*, *13*, 1093–1104, 1983.
- Hogan, P. J., H. E. Hurlburt, G. A. Jacobs, A. J. Wallcraft, W. J. Teague, and J. L. Mitchell, Simulation of GEOSAT, TOPEX/Poseidon, and ERS-1 altimeter data from a $1/8^\circ$ Pacific Ocean model: Effects of space-time resolution on mesoscale sea surface height variability, *Marine Technology Society Journal*, *26*(2), 98–107, 1992.
- Hurlburt, H. E., and J. D. Thompson, A numerical study of the Loop Current intrusions and eddy-shedding, *Journal of Physical Oceanography*, *10*, 1611–1651, 1980.
- Hurlburt, H. E., and J. D. Thompson, The dynamics of the Loop Current and shed eddies in a numerical model of the Gulf of Mexico, in *Hydrodynamics of Semi-enclosed Seas*, edited by J. C. J. Nihoul, 243–298, Elsevier Scientific Publishing Company, Amsterdam, 1982.
- Hurlburt, H. E., and J. D. Thompson, Preliminary results from a numerical study of the New England Seamount Chain influence on the Gulf Stream, in *Predictability*, Company, Amsterdam, 1982.
- Hurlburt, H. E., and J. D. Thompson, Preliminary results from a numerical study of the New England Seamount Chain influence on the Gulf Stream, in *Predictability*

- of fluid motions*, edited by G. Holloway and B. J. West, 489–503, American Institute of Physics, New York, 1984.
- Hurlburt, H. E., A. J. Wallcraft, Z. Sirkes, and E. J. Metzger, Modeling of the Global and Pacific Oceans: On the path to eddy-resolving ocean prediction, *Oceanography*, 5, 9–18, 1992.
- Hurlburt, H. E., A. J. Wallcraft, W. J. Schmitz Jr., P. J. Hogan, and E. J. Metzger, Dynamics of the Kuroshio/Oyashio current system using eddy-resolving models of the North Pacific Ocean, *Journal of Geophysical Research*, 101, 941–976, 1996.
- Jacobs, G. A., W. J. Teague, J. L. Mitchell, and H. E. Hurlburt, An examination of the North Pacific Ocean in the spectral domain using Geosat altimeter data and a numerical ocean model, *Journal of Geophysical Research*, 101, 1025–1044, 1996.
- Levitus, S., Climatological atlas of the world ocean, *NOAA Professional Paper-13*, 173 pp., 1982.
- Mattsson, J., Observed linear flow resistance to the öresund due to rotation, *Journal of Geophysical Research*, 100, 20,779–20,791, 1995.
- Messinger, F., and A. Arakawa, *Numerical Methods Used in Atmospheric Models*, GARP Publ. Serv., World Meteorological Organization, 64 pp., 1976.
- Metzger, E. J., and H. E. Hurlburt, Coupled dynamics of the South China Sea, the Sulu Sea and the Pacific Ocean, *Journal of Geophysical Research*, 101, 12331–12352, 1996.
- Metzger, E. J., H. E. Hurlburt, J. C. Kindle, Z. Sirkes, and J. Pringle, Hindcasting of wind-driven anomalies using a reduced gravity global ocean model, *Journal of the Marine Technology Society*, 26(2), 23–32, 1992.
- Mitchell, J. L., W. J. Teague, G. A. Jacobs, and H. E. Hurlburt, Kuroshio Extension dynamics from satellite altimetry and a model simulation, *Journal of Geophysical Research*, 101, 1045–1058, 1996.
- Munch, C. L., The effect of the Hawaiian Ridge on mesoscale variability: results from TOPEX/Poseidon, Master's thesis, University of Hawaii, 1996.
- Munk, W. H., On the wind driven ocean circulation, *Journal of Meteorology*, 7, 79–93, 1950.
- Mysak, L. A., and L. Magaard, Rossby wave driven Eulerian mean flows along non-zonal barriers, with application to the Hawaiian Ridge, *Journal of Physical Oceanography*, 13, 1716–1725, 1983.
- Mysak, L. A., and L. Magaard, Rossby wave driven Eulerian mean flows along non-zonal barriers, with application to the Hawaiian Ridge, *Journal of Physical Oceanography*, 13, 1716–1725, 1983.

- NOAA, ETOP05 digital relief of the surface of the earth, Natl. Geophys. Data Cent., Washington, D.C., data Announce. 86-MGG-07, 1986.
- Oh, I. S., and L. Magaard, Rossby wave-induced secondary flows near barriers, with application to the Hawaiian Ridge, *Journal of Physical Oceanography*, *14*, 1510–1513, 1984.
- Price, J. M., M. L. Van Woert, and M. Vitousek, On the possibility of a ridge current along the Hawaiian Islands, *Journal of Geophysical Research*, *99*, 14101–14111, 1994.
- Qiu, B., D. A. Koh, C. Lumpkin, and P. Flament, Existence and formation mechanism of the North Hawaiian Ridge Current, *Journal of Physical Oceanography*, *27*, 431–444, 1997.
- Shriver, J. F., and H. E. Hurlburt, The contribution of the global thermohaline circulation to the Pacific to Indian Ocean throughflow via Indonesia, *Journal of Geophysical Research*, *102*, 5491–5511, 1997.
- Sun, L. C., J. M. Price, L. Magaard, and G. I. Roden, The North Hawaiian Ridge Current: a comparison between analytical theory and some prior observations, *Journal of Physical Oceanography*, *18*, 384–388, 1988.
- Sverdrup, H. U., Wind driven currents in a baroclinic ocean: with application to the equatorial currents of the Eastern Pacific, in *Proceedings of the National Academy of Science*, vol. 33, U.S.A., 1947.
- Talley, L. D., and R. A. DeSzoek, Spatial fluctuations north of the Hawaiian Ridge, *Journal of Physical Oceanography*, *16*, 981–984, 1986.
- Wallcraft, A. J., *The Navy Layered Ocean Model user's guide*, Nav. Res. Lab, Stennis Space Center, Miss., 21 pp., 1991.
- White, W. B., A narrow boundary current along the eastern side of the Hawaiian Ridge; the North Hawaiian Ridge Current, *Journal of Physical Oceanography*, *13*, 1726–1731, 1983.
- Wyrtki, K., Sea level and the seasonal fluctuations of the equatorial currents in the Western Pacific Ocean, *Journal of Physical Oceanography*, *4*, 91–103, 1974.

BIOGRAPHICAL SKETCH

The year was 1972, the day was December 10th. Aside from it being the day the Apollo 17 Spacecraft was injected into lunar orbit before landing on the moon on December 11th, it was also the day on which I was brought into this world by a wonderful physician in a small town (Crystal Falls) in northern Michigan. It was exactly 31 years after the Japanese invasion of the Philippines and 22 years after William Faulkner accepted the Nobel prize.

I was born unto two wonderfully caring parents, Gregory Alan (my namesake) and Hollis Marie (Haun). It has been said that I was an unusually quiet baby. My parents have been wondering what may have changed this since I began to talk. Growing up in Sturtevant, a small town in southeastern Wisconsin, was eventful to say the least. I managed to get into all sorts of mischief while still being able to learn a great appreciation for all of the wonders of nature that surrounded me. All through the course of my formative years I was into trouble and caused many headaches for my parents and my brother Scott.

As a preteen I took my first stab at a job, I became a paper boy. What a fun experience. I had the thrill of seeing the town, the ability to make money, and the time to think. You could say it was the beginning of my more philosophical side. As soon as the teenage years rolled around, the thrill of making money and playing by the rules had subsided. It was that time in every boys life where he feels he needs to stick it to THE MAN. Needless to say, my parents were not pleased with me, and I now realize the trouble that I was.

stick it to THE MAN. Needless to say, my parents were not pleased with me, and I now realize the trouble that I was.

Such as it may be, that phase soon passed, much to the chagrin of my parents, and I once again dove into the working world. Aah, capitalism, the only system in which a 15 year old can get hired on as slave labor at the local fast food place and have to fork over money to the government in taxes. Funny how in this democratic country of ours, you must begin to pay taxes into the system before you are allowed to vote on the system in which you are trapped.

Soon began a new chapter in my life, the onset of both high school and puberty. Being a person who likes variety and excitement, I of course chose activities in high school that didn't really place me in any one particular social category. As such, I had a wide variety of friends and many open minded lessons in life. I cherish them to this day. Academically, I took classes as every other kid did. I did well in them, but never excellent. Sure, the potential was there, and did I hear it from everyone and their brother, but I was generally bored with school and chose to try to entertain myself (and others). In retrospect, this was not a wise thing to do since it led to all sorts of trouble and trips to the principles office, but then again, I really had no control over my boredom. I was the product of a system that strived to produce a heterogeneous pool of mediocre individuals that all had the same talents, same faults, and same ambitions. The social programming which I despise began long ago.

I also took my shot at sports in high school participating in both football and golf. Football was something I was destined for being a big kid, but something I would never be great at due to my passive nature and fear of pain. I was good, but not great. I also lacked the ambition to improve myself muscularly due to the sudden onset of boredom imposed by lifting weights. Golf, on the other hand, was a game I had never played and decided to try just so I could learn it. I began as a horrible golfer, got better, but was never destined to be great due to my complete frustration I had never played and decided to try just so I could learn it. I began as a horrible golfer, got better, but was never destined to be great due to my complete frustration

and lack of control of the golf ball. Golf, such as it was, remains to be an entertaining but ever frustrating sport.

I was also in the high school band and jazz band, playing the tenor saxophone. A lovely instrument, I cherished the moments in Jazz when my classmates and myself would be able to just sit around and jam with the instructor. Our teacher was one of the best I ever had. He taught us the true meaning of letting go through music and implanted into our hearts and souls the love for rhythm, variation, and spontaneity.

After high school, I decided to attend the University of Wisconsin in Madison. It was close enough to home to see my parents, yet far enough away to feel independent and get a taste for life. In Madison, I excelled in my meteorology program while maintaining a healthy (sometimes not too healthy) social life and participating in a university club sport, rugby. The mix between learning, socializing, and athletics proved to be the perfect recipe for my happiness. After four years of undergraduate education and off season construction work, I graduated with a Bachelor of Science in Meteorology.

In the final year of my undergraduate training, I began to sense the need for something more. I needed something higher and harder to motivate me. I needed more education in a highly disciplined field. I decided to attend The Florida State University and pursue a career in Physical Oceanography. I accepted a Naval Research laboratory fellowship and moved to Tallahassee, Florida, in the summer of 1995. I have been here ever since.